Journal of Instrumentation

Vibrating wire monitor: Versatile instrumentation for particle and photon beam measurements with wide dynamic range

Jinst

Published by IOP Publishing for Sissa Medialab

Received: *July 27, 2020*
Accepted: *November 6, 2020*
Published: *January 4, 2021*

Review

Vibrating wire monitor: Versatile instrumentation for particle and photon beam measurements with wide dynamic range

S.G. Arutunian,[a,1] **A.V. Margaryan,**[a] **G.S. Harutyunyan,**[a] **E.G. Lazareva,**[a] **M. Chung,**[b] **D. Kwak**[b] **and D.S. Gyulamiryan**[c]

[b] *Alikhanyan National Scientific Laboratory, 0036 Yerevan, Armenia*
[b] *Ulsan National Institute of Science and Technology, 44919 Ulsan, South Korea*
[c] *Quantum College, 0046 Yerevan, Armenia*

E-mail: femto@yerphi.am

Abstract: The vibrating wire monitor proposed herein is based on the strong dependence of the frequency of the pinched wire on its temperature. This dependence allows the measurement of a particle/X-ray/gamma-ray beam that deposits part of its energy on the wire. A wide measured temperature range from fractions of mK to hundreds of degrees allows the detection of beam properties at a given position of the wire in space. It also enables preparing profiling of a beam in a large dynamic range by scanning the wire through the beam. This review paper presents information on various applications of a vibrating wire, including the method of resonance target and the use of wire oscillations as a scanner for the profiling of thin beams.

Keywords: Beam-line instrumentation (beam position and profile monitors; beam-intensity monitors; bunch length monitors); Instrumentation for particle accelerators and storage rings - high energy (linear accelerators, synchrotrons); Instrumentation for particle accelerators and storage rings - low energy (linear accelerators, cyclotrons, electrostatic accelerators); Instrumentation for synchrotron radiation accelerators

[1]Corresponding author.

https://doi.org/10.1088/1748-0221/16/01/R01001

2021 JINST 16 R01001

Contents

2021 JINST 16 R01001

1 Introduction

Using particle or photon beams frequently requires information on the beam intensity in the beam cross-section. For two-dimensional (2D) profiling, generally, techniques based on screens are used. The most direct approach of beam observation is to detect the light emitted from the scintillation screen by a CCD camera (see e.g., [1–3]). When a charged particle penetrates a material, the energy loss can be transformed into fluorescence light. The screen is observed by a CCD camera. Crystal scintillation screens are frequently used as scintillation materials. Standard scintillation materials used for imaging screens include YAG:Ce, LuAG:Ce (ideal for consecutive photodiode and avalanche photodiode readout), and YAP:Ce (suitable for readout in the ultraviolet range) [4].

Optical transition radiation (OTR) monitors are also extensively used for profile measurements. They are thin reflecting screens, such as silicon wafers covered with a thin layer of aluminum or silver in vacuum [5]. Compared to scintillator screens, which are typically approximately 1 mm thick, OTR has the advantage of being achieved from very thin foils, with much less scattering of

beam particles, and therefore, less emittance increase. OTR is emitted from both sides of a foil. In contrast to OTR, scintillation light is emitted isotropically, i.e., there is no restriction on the observation geometry, and both the screen and the camera can be positioned at arbitrary angles with respect to each other [5]. In circular accelerators, synchrotron radiation is frequently used as a 2D replica of the beam profile. For diagnostic purposes, light is extracted from an accelerator and transported to a measuring equipment via various optical elements, such as windows, mirrors, lenses, and fibers. The receivers are TV cameras, CCDs, photodiodes (single or in an array), etc. [6].

For low-current beam diagnostics, scintillating crystals have larger signal-to-noise ratio than OTR screens or wire scanners, and, therefore, are extensively used. For example, in accelerator AREAL YAG:Ce scintillation screens of $30 \times 30\,\mathrm{mm}^2$ and 20-µm thick are installed for profile measurements [7]. However, in ref. [8], saturation of scintillating spots in the YAG:Ce crystal was noticed. Saturation becomes a relevant issue at beam intensities of the order of $\sim 0.04\,\mathrm{pC/\mu m}^2$ for a 100-MeV beam, and this limit scales with energy, being inversely proportional to the beam energy loss function.

Another extensively used profiling method is scanning the electron or hadron beam with a thin wire (see reviews [9–13]). Information on the number of particles or photons that intersect the wire is determined by the intensity of the secondary particle or radiation flow generated by the interaction of primary particles with the wire material. The advantage of the above method is the low impact of the measuring tool on the beam. Its disadvantage is that each scan provides information about only the one-dimensional profile of the beam (the wire integrates the contributions of all the particles along its length). In addition for high-energy beams, the flow of secondary particles/radiation is directed along the propagation direction of the measured beam and requires installation of an additional measurement system far from the interaction area, typically outside the vacuum chamber in the case of accelerators. For detailed descriptions of wire scanners for electron beam profiling see reference [13]. A typical wire scanner for hadron beam measurement is described in [14] (speed of scan less than 1 m/s). Special fast wire scanners have been developed to decrease the scanning time (see e.g. [15, 16]) (speed of scan up to 20 m/s). Note the trend in the development of wire scanners with very short wires using nanofabrication technologies, designed to measure beams with sizes smaller than a few hundred microns [17, 18]. Instead of measuring the flow of the scattered particles from the wire, a method has been developed to measure the secondary current generated by electron emission from the wire (see [10, 11] for an introduction to the method). In this case, the wire material must be conductive. The secondary emission signal is typically used with low-energy beams as in this case no energetic secondary particles are generated [10]. Monitors based on such principle are highly compact and require analogue measurements of small currents [1].

In [8], different methods of profiling are compared. Scintillation YAG:Ce crystals of different thicknesses, an OTR screen, a phosphor screen, and a wire scanner (see also [19]) were used to measure the beam profile at the ATF photo-injector facility (a single-pulse photoelectron beam of 1 nC, with energy of 66 MeV). A significant sized blurring was observed on both YAG:Ce crystals and the phosphor screen compared to that on the OTR screen and wire scanner. The recorded results presented quite different full width at half maximum (FWHM) values: 380 µm for 0.5-mm YAG, 320 µm for 0.25-mm YAG, 300 µm for phosphor screen, 175 µm for the OTR screen, and 185 µm for the wire scanner (see also [20]).

2021 JINST 16 R01001

To address some of the limitations in the conventional beam instrumentation for accelerators, vibrating wire sensors and monitors have been developed since 1999 [21]. The operating principle of these sensors is based on the measurement of the change in the frequency of a vibrating wire as a function of the wire temperature. Instead of exciting traditionally used steel wires in the transverse vibration using an electromagnet, the interaction of the AC current through a vibrating wire with a permanent magnet is employed. This allows using non-steel wires and maintaining very stable wire oscillations (less than 0.005-Hz variation in a 5000-Hz full range). In accelerator diagnostics, vibrating wire monitors (VWMs) are mainly aimed at measuring the transversal profiles of different types of beams. The thermal principle of operation allows measuring charged particles, photons in a wide range of wavelengths, and even neutrons [22, 23]. It should also be noted that the inherent long-term reliability, minimum zero drift, and signal immunity to electrical noise are of prime importance [24].

2 Physical fundamentals of vibrating wire method

2.1 Vibrating wire resonator and autogeneration principle

The operating principle of diverse vibrating wire sensors is based on the measurement of a change in the frequency of the vibrating wire that is stretched on a support, as a function of the physical parameters of the wire and the environment in which the oscillations occur. There are numerous different types of vibration wire sensors (see e.g., [24]):

- In the permanent excitation method, an electrical energy impulse maintains sufficient energy in the wire for its permanent vibration.
- In the resonance method, typically two electromagnets are used. The first one acts as an actuator, whereas the second one serves as a sensor for the oscillation frequency observation.
- In the impulse method, an electromagnet serves as a shock actuator as well as a velocity sensor. An electrical impulse through an electromagnetic coil applies a very brief point force on the wire. After some time, the first mode component of the free response dominates.

As a background of the development, we use an electromechanical resonator with a vibrating metallic wire that is excited by the interaction of a current with a permanent magnetic field.

The automatic generation of vibrations at the natural frequency of the wire is achieved using a feedback electronic circuit (see below for more details) with a system for stabilizing the amplitude of the vibrations of the wire. This is important because a wire is essentially a nonlinear object, and its frequency can vary not only under the influence of the measured beam but also with the variations in the amplitude of the wire oscillations.

Advantages of the technology of permanent excitation of oscillations are noted in [24]; these include compactness of the magnets (leading to sensor volume reduction) and enhanced robustness. Our studies have shown that structures with permanent excitation of oscillations using magnets also have the following benefits. After a certain period when the sensor enters the operating mode, stable and flat single-harmonic oscillations are generated in the system. Simultaneously, the entire ensemble at the output of the autogeneration circuit continues to present the natural frequency of the wire oscillations, even under rapid variation.

2021 JINST 16 R01001

A schematic of a typical vibrating wire resonator [25] is presented in figure 1. The resonator can be roughly represented as a support with a strained vibrating wire. Special clamps rigidly fasten the ends of the wire, so that its length is strictly defined by the distance between these clamps (the base is much more rigid than the wire).

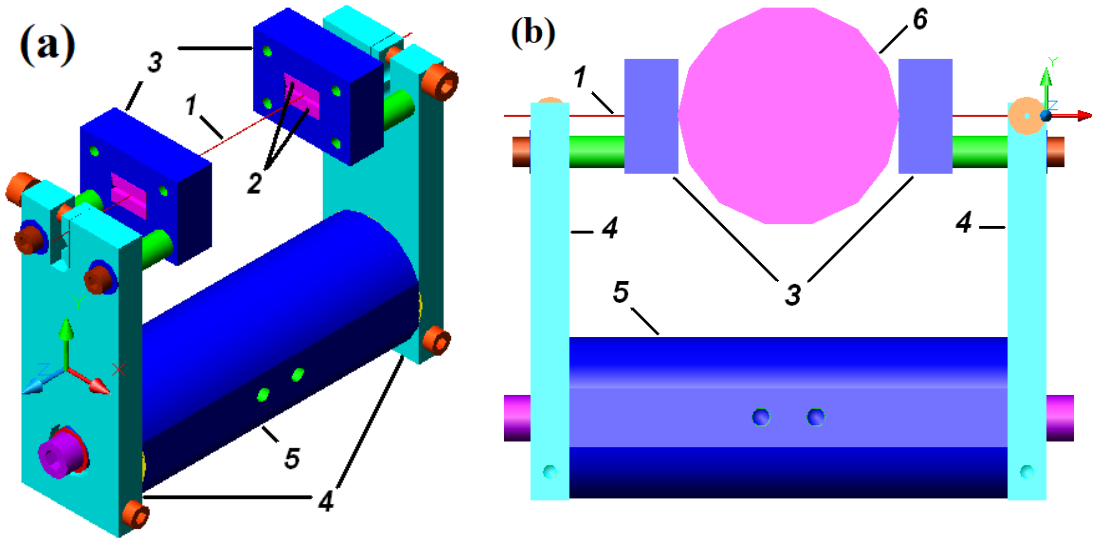

Figure 1. (a) Main view of monitor with aperture of 40 mm and wire length of 80 mm: 1 — vibrating wire, 2 — magnets, 3 — magnet poles, 4 — clamps, 5 — basis. (b) Aperture of monitor is defined by circle 6 placed between magnet poles.

The scheme of the autogeneration of natural oscillations of the wire is presented in figure 2. The basis of the oscillation generation process is the amplification of the random vibrations of the wire. The wire is connected to a positive feedback circuit, so that the mechanical fluctuations on the wire generate an electromotive force(emf) pulse that is amplified and transmitted to the wire in the same phase. Because the attenuation of the oscillations is minimal in response to the natural frequency of the circuit, the resonant frequency that is selected by the feedback circuit is equal to the natural frequency of the wire. The electrical signal from the wire is actually that at the output of the operational amplifier in the feedback circuit (OP1 output in figure 2). We also added an important system for stabilizing the amplitude of the generated oscillations.

The process of autogeneration is complex and defined by all the parameters of the sensor resonator as well as the circuit and values of the electronic components in the scheme of autogeneration. The former are the diameter and length of the wire, material of the wire, structure of the magnetic field including the distribution of the magnetic field along the wire, and value of the magnetic field in the area of the wire. The magnetic field is determined by the type of permanent magnets used and the size of the magnetic pole gap. Accordingly, the process of starting vibrations at the natural frequency is significantly different for different types of sensors. It should be noted that in [26], the resonator, consisting of a vibrating wire, its mounting system, and the magnetic field, is interpreted as an equivalent electrical circuit comprising an inductor, a resistor, and a capacitor (see also [27–29]). Such a replacement of the resonator by an equivalent unit of electronic components allows to effectively select component values of the autogeneration scheme (see figure 3).

2021 JINST 16 R01001

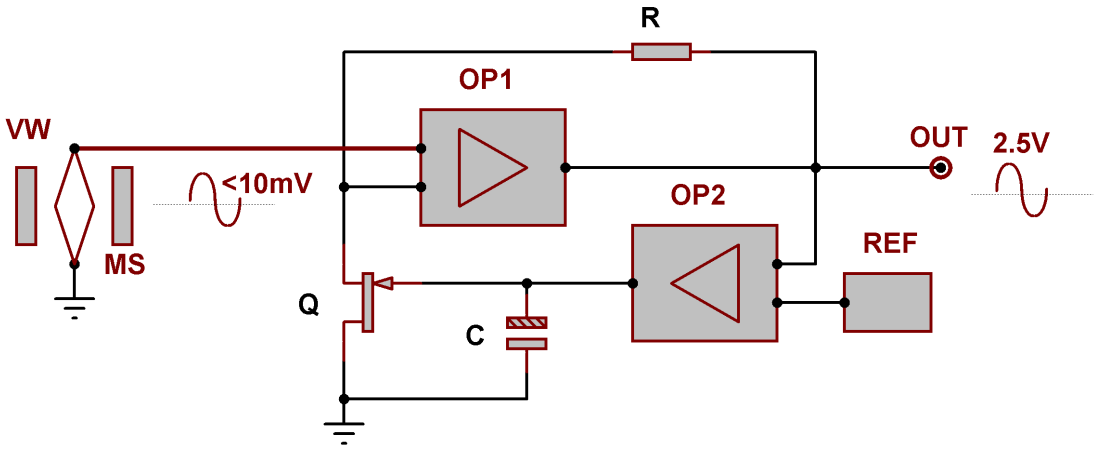

Figure 2. Automatic generation board of natural oscillations of wire (schematically). VW — vibrating wire, MS — magnetic system, OP1 — main operational amplifier unit, OP2 — operational amplifier unit in wire oscillation amplitude stabilization circuit, REF — voltage reference source that regulates oscillation amplitude, Q — field transistor in circuit of wire vibration amplitude stabilization, OUT — output signal, R — resistor, whose nominal value is selected depending on parameters of resonator, C — capacitor that adjusts process of signal stabilization depending on frequency range of oscillations.

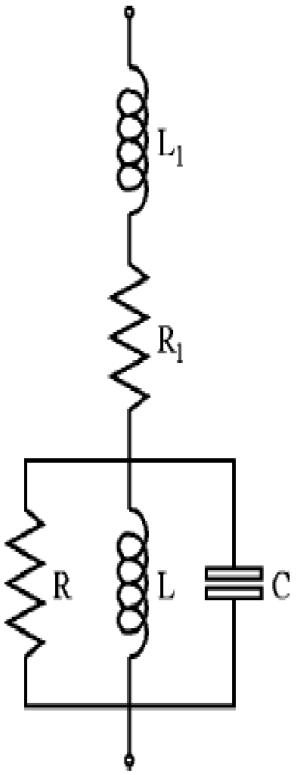

Figure 3. Electronic lumped-parameter RLC circuit equivalent to vibrating wire resonator [26] (a parallel RLC oscillating circuit can be considered an electrical analog of the mechanical oscillator, in which R_1 and L_1 describe electrical properties of the wire and leading-in cable).

2.2 Resonator and magnetic field selection

The selection of the vibrating wire resonator is governed by the specific application of the monitor. The standard VWM consists of a single wire, wire clamps, and a magnetic field system, as shown in figure 1. The space along the wire is almost half occupied by the magnetic field, which reduces the aperture of the sensor. In some cases, resonators with the largest possible aperture are required, to measure beams with a large transverse beam size. For this purpose, several variants of such large-aperture monitors have been developed on the yoke principle [30–32]. This type of a VWM has two mechanically coupled wires (vibrating and target). Coupling is maintained by a special balancing arm (yoke). Such a monitor has a much larger aperture size than previous VWM models. A prototype of such a large-aperture VWM with a target wire length of 60 mm was designed, manufactured, and bench-tested on a proton beam of Fermilab High Intensity Neutrino Source facility (with proton energy of 2.5 MeV and average beam current of 0.01–2.8 mA [31]) (see figure 4).

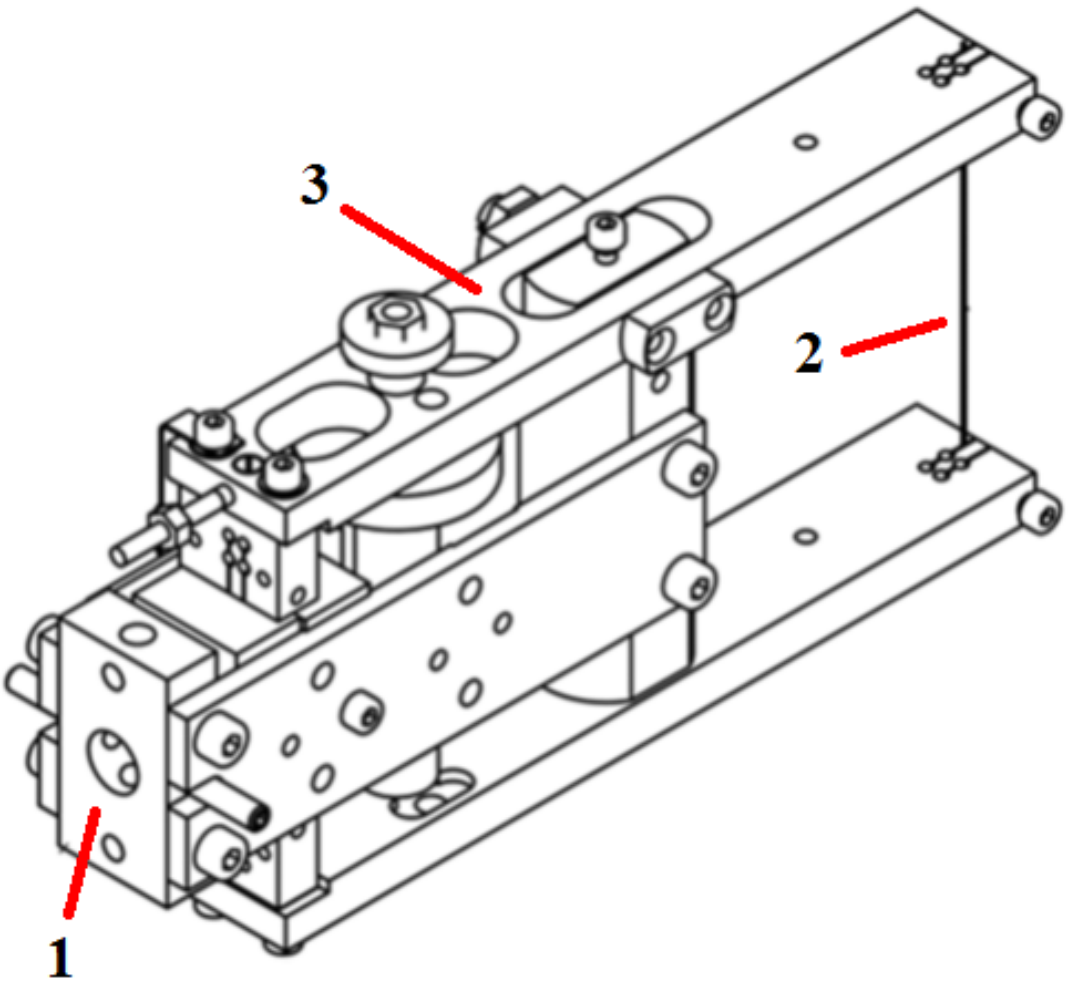

Figure 4. Yoke-type vibrating wire resonator: 1 — vibrating wire assembly, 2 — target wire, 3 — balancing arm (yoke) coupling vibrating and target wires.

Multi-wire sensors with a system of vibrating wires have also been produced. Such sensors allow measurement of a beam profile at the corresponding number of points without scanning the beam. Monitors with five wires were manufactured and used to measure the undulator and synchrotron radiations at the Advanced Photon Source of Argonne National Laboratory (APS-ANL) [33, 34] (see below for more details).

For some applications (e.g., for thin-beam profiling, where the vibrating wire plays the role of a miniature scanner), it is desirable to increase the amplitude of the oscillation of the wire, i.e., to increase the sweeping area of the wire during its oscillation. This could be realized by increasing the autogeneration current in the oscillation excitation circuit. However, this is not desirable, because of the consequent increase in the degree of nonlinearity in the oscillations of the wire. For the development stage of the method of thin-beam profiling using a vibrating wire [35, 36], the sinusoidality of the oscillations needs to be maintained, which would permit precisely defining the position of the wire in space. Therefore, as an alternative, we increased the length of the wire. A model resonator with a length of 120 mm and a movable magnetic field system was developed. The design of such a resonator with a magnetic field created by a pair of magnetic poles (11 mm in width) with permanent magnets of diameter 10 mm and thickness 5 mm is shown in figure 5. Specifically, the resonators discussed here are aimed at the excitation of the flat oscillations of a wire. The problem is that the frequencies of natural vibrations in two orthogonal transverse directions differs slightly, because of ovality of the wire and asymmetry in the fastening at its ends. Nonflatness of the oscillations may arise, owing to the defects in the manufacturing and alignment of the magnetic system components. For studying completely mixed oscillations in transverse directions in this resonator, it is possible to rotate two units of the magnetic system by 90° from each other (see figure 5(b)).

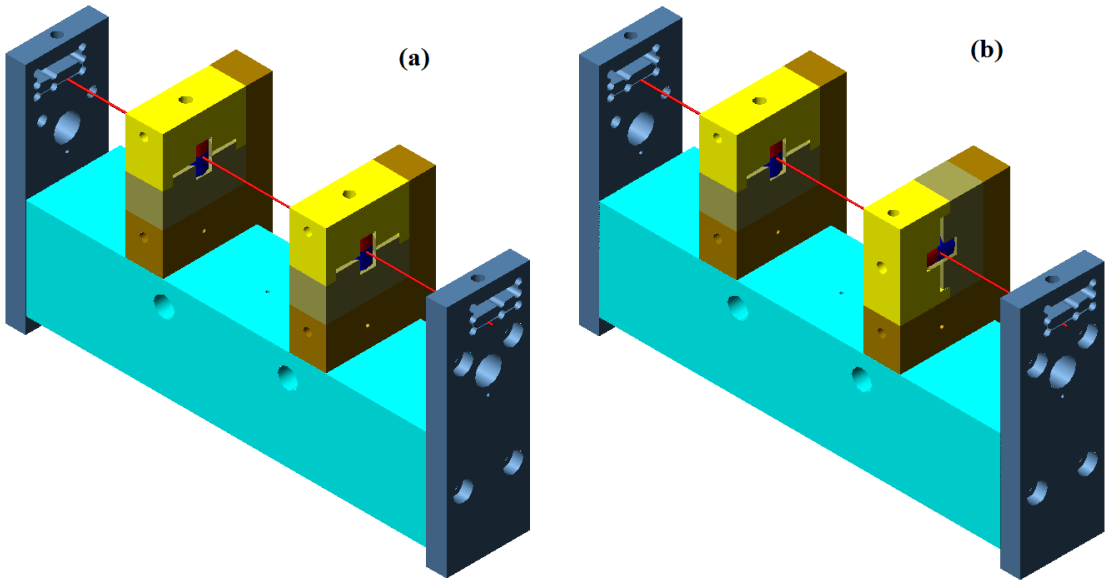

Figure 5. Vibrating wire resonator design with wire length of 120 mm for studying influence of magnetic system on wire oscillations: (a) planes of two units of magnetic system coincide, (b) planes of two units are orthogonal to each other.

2021 JINST 16 R01001

Note that in resonators in which the magnetic field covers only a small part of the length of the wire, there is a probability that several harmonics may be excited simultaneously. For the resonator shown in figure 5(a), the distribution of the magnetic field is presented in figure 6. As can be seen, this arrangement of magnetic poles practically excludes the generation of the third-harmonic oscillations; however, it is favorable for the excitation of the first and fifth ones i.e., oscillations tend to be excited if the magnetic field and the corresponding force on the wire are concentrated in the region of oscillation antinodes, and conversely if the magnetic field is concentrated near oscillation nodes, oscillations are not easily excited.

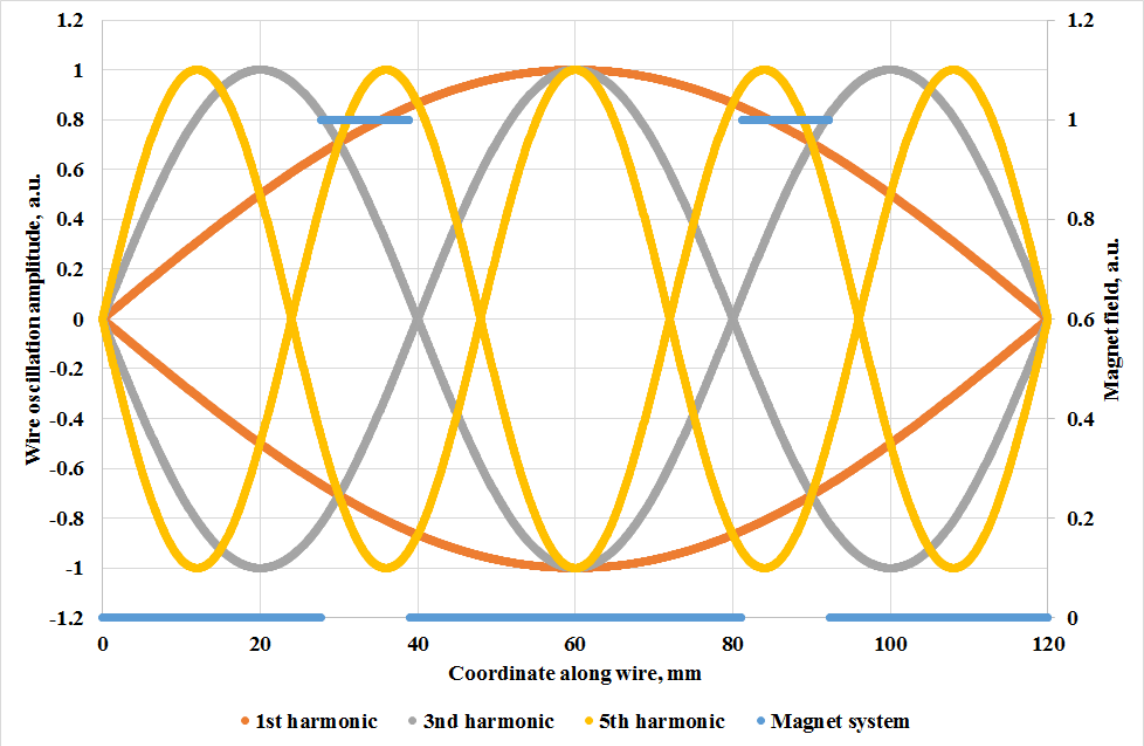

Figure 6. Magnetic field and oscillation harmonics of vibrating wire resonator with length of 120 mm. Blue line — distribution of magnetic field along wire, orange — first-harmonic oscillations of wire, grey — third-harmonic oscillations, yellow — fifth-harmonic oscillations.

Below are some results obtained using a model resonator with a 120-mm wire length for various modifications of the autogeneration boards. The measurements were made with a RTB2004 oscilloscope. The results of the autogeneration process of the natural oscillations for the StrGen DVW_2018 board with operational amplifiers in the SMD version and capacitor C = 3300 nF (see figure 2) are presented in figure 7. An interesting feature was noted: the autogeneration process began with the generation of the fifth-harmonic oscillation, which after a reasonably long time (approximately 10 s) was regenerated in the production of the first harmonic in the form of an admixture of oscillations. The fraction of the fifth harmonic depended on the features of the electronic components of the autogeneration board and the values of the key resistors and capacitors.

Figure 8 shows a similar process of oscillation generation of the same resonator with an StrGen V4.1USB board, which used operating amplifiers in the DIP version and capacitor C = 220 nF.

2021 JINST 16 R01001

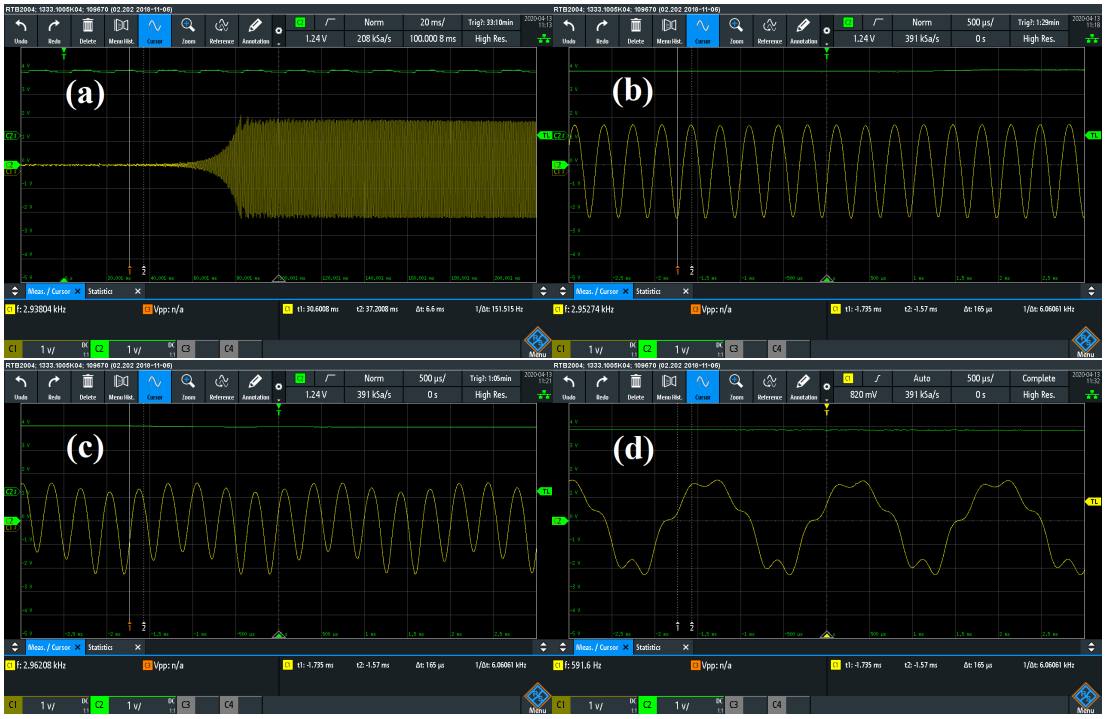

Figure 7. Autogeneration process using 120-mm wire length monitor, autogeneration board StrGen DVW_2018 with operational amplifiers in SMD version, and capacitor $C = 3300\,\text{nF}$. (a) Because of high capacitor values in feedback circuit, autogeneration process starts after approximately 3 s, and the fifth harmonic is generated. Horizontal scale of the oscilloscope waveform is 20 ms per division. (b) Fifth harmonic sustains for sufficiently long time (up to 5 s). Horizontal scale of the oscilloscope waveform is 500 µs per division. (c) Subsequently, together with the fifth harmonic, first harmonic (12 s) increases. Horizontal scale of the oscilloscope waveform is 500 µs per division. (d) System enters stationary mode (over 30 s), with a mixture of first and fifth harmonics, in which fifth harmonic is important. Horizontal scale of the oscilloscope waveform is 500 µs per division.

2.3 Frequency dependence on wire temperature

The interaction of the beam with the wire mainly causes the wire to heat. The corresponding change in the natural oscillation frequency of the wire provides information about its temperature and accordingly the number of particles/photons of the beam penetrating the wire.

At the assembly temperature (T_0), the tension of the wire is defined using the length between the clamps mounted on the base, L_B^0 (bed length) and the non-tensioned wire length, L_W^0 as follows:

$$\sigma_0 = \frac{L_B^0 - L_W^0}{L_W^0} E_W = \frac{\Delta L_W^0}{L_W^0} E_W, \tag{2.1}$$

where E_W is the elasticity modulus of the wire material.

The frequency of the second harmonic of the wire oscillations can be expressed as

$$F_0 = \frac{1}{L_B^0} \sqrt{\sigma_0/\rho}, \tag{2.2}$$

where ρ is the density of the wire material.

2021 JINST 16 R01001

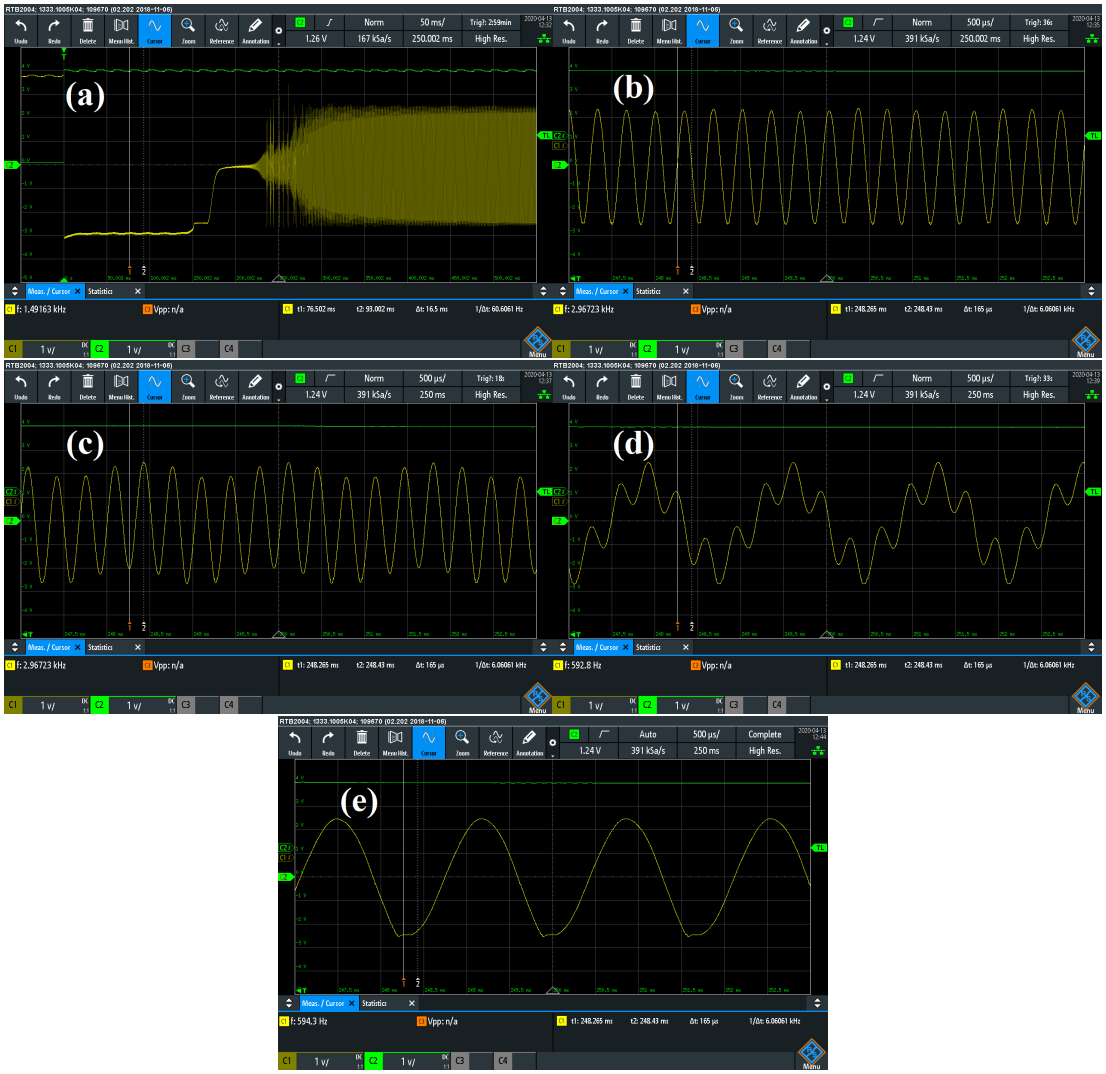

Figure 8. Autogeneration process using 120-mm wire length monitor, autogeneration board StrGen V4.1USB with operating amplifiers in DIP version, and capacitor $C = 220\,\text{nF}$. (a) Because of low capacitor values, the generation process starts early. Horizontal scale of the oscilloscope waveform is 50 ms per division. (b) Similar to previous case, initially fifth harmonic is generated. Horizontal scale of the oscilloscope waveform is 500 µs per division. (c) Appearance of fifth harmonic after 1 s. Horizontal scale of the oscilloscope waveform is 500 µs per division. (d) Subsequently, first harmonic starts to increase (5 s). Horizontal scale of the oscilloscope waveform is 500 µs per division. (e) After 10 s, the first harmonic sustains, with slight distortion of sinusoidal oscillations near extremes, probably due to admixing of fifth harmonic. Horizontal scale of the oscilloscope waveform is 500 µs per division.

Let us assume that the wire is heated by ΔT (ambient temperature and temperature of the base remain unchanged). The corresponding change in the wire density yields

$$\frac{\Delta\rho}{\rho} = -3\alpha_W \Delta T, \tag{2.3}$$

where α_W is the linear expansion coefficient of the wire.

2021 JINST 16 R01001

Because the length of the wire is determined by the distance between the attachment points on the base (bed length), it is L_B^0 and does not change. However, the tension in the wire varies, owing to changes in the length of the wire in the non-tensioned state. We have

$$\frac{\Delta L_W}{L_W^0} = \alpha_W \Delta T, \tag{2.4}$$

and correspondingly,

$$\Delta\sigma = E_W \frac{L_W^0}{L_B^0} \alpha_W \Delta T, \tag{2.5}$$

and accordingly,

$$\frac{\Delta\sigma}{\sigma_0} = \frac{E_W}{\sigma_0} \frac{L_W^0}{L_B^0} \alpha_W \Delta T. \tag{2.6}$$

The process of tensioning the wire when only its temperature changes is illustrated in figure 9.

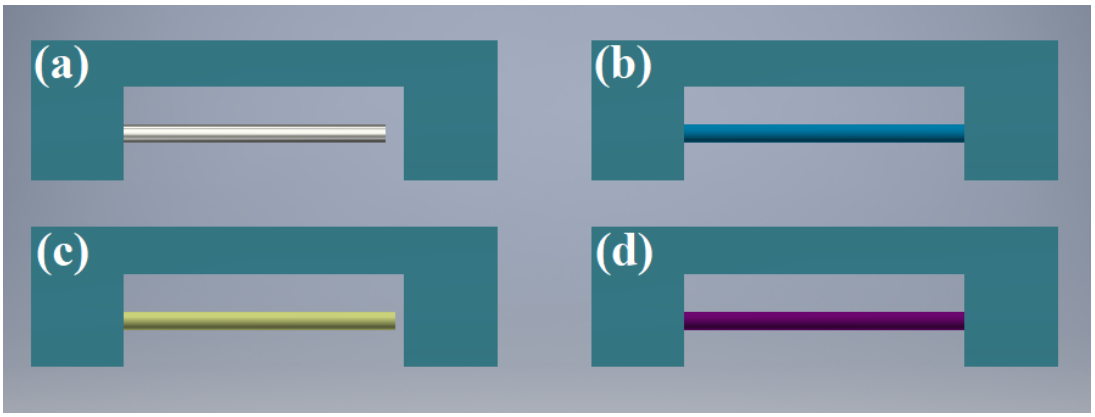

Figure 9. Tensioning wire when only its temperature changes. (a) Base (cadet blue) — length of bed for wire $L_B^0 = 30\,\text{mm}$, wire (silver) — length in non-tensioned state $L_W^0 = 28\,\text{mm}$. (b) Wire (sky blue medium) is stretched on bed length of base and becomes $L_B^0 = 30\,\text{mm}$, i.e., tension of wire is calculated using $\Delta L_W^0 = 2\,\text{mm}$. (c) For base, temperature does not change, i.e., bed length remains 30 mm, whereas on heating, length of wire (satin lemon chiffon) in non-tensioned state increases to $L_W = L_W^0(1 + \alpha_W \Delta T) = 29\,\text{mm}$. (d) Wire (smooth purple) is stretched along bed length of base and becomes 30-mm long, i.e., wire tension is calculated using $\Delta L_W = 1\,\text{mm}$.

The values of the expansion coefficients of metals are in the range of a few units of 10^{-6}–$2 \times 10^{-5}\,\text{K}^{-1}$ Thus, at a temperature shift of 1 K, the relative changes in both the length and density are approximately 10^{-5}. Under tension, based on eq. (2.6), there is an additional factor, E_W/σ_0, which is very large. For example, for stainless steel (AISI 316), $E_W = 190$–$210\,\text{GPa}$ and the tensile strength is 460–860 MPa. The initial tension on the wire was taken as 30%–70% of the tensile strength (assumed to be 700 MPa for the VWM wire), so that E_W/σ_0 is approximately 400. From these simple estimations one can see that the temperature dependence of ρ is negligible compared to that of the tension. As a first approximation, one can also neglect the difference between L_B^0 and L_W^0, so that without causing any misunderstanding we can use $L_W^0 \approx L_B^0 \approx L$. To summarize, we obtain the formula for frequency

$$F = \frac{1}{L}\sqrt{(\sigma_o - E_W \alpha_W \Delta T)/\rho}. \tag{2.7}$$

2021 JINST 16 R01001

Figure 10 presents the temperature dependence of the frequency and sensitivity of the resonator utilizing the vibrating wire.

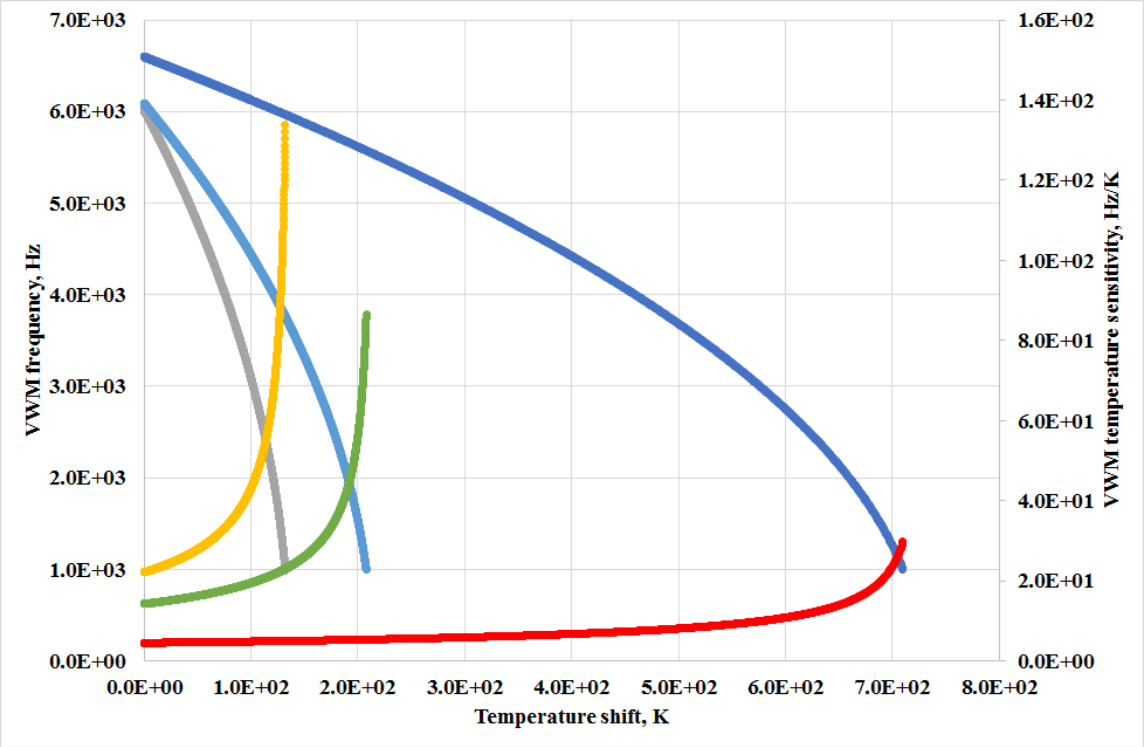

Figure 10. Frequency of vibrating wire and sensitivity of monitor to overheating of wire as functions of temperature of assembly with wires formed of tungsten (frequency — dark blue, sensitivity — red), beryllium bronze (Beryllium Bronze — Cu97.5/Be2/Co-Ni0.5, UNS C17200) (frequency — blue, sensitivity — green), and stainless steel (AISI 316) (frequency — gray, sensitivity - yellow). Sensitivity of monitor is slope of frequency versus temperature relation. In all three cases, it is assumed that during assembly, wire is stretched by 70% of the strength of material.

Table 1 contains mechanical parameters of wire materials (for tungsten and stainless steel, data are taken from [37] and for bronze from [38]), and values of initial tension and corresponding frequency of VWM.

Table 1. Mechanical parameters of some wire materials and corresponding initial characteristics of VWM. Here, σ_{TS} is the tensile strength.

	E_W GPa	σ_{TS} MPa	ρ kg/m^3	α_W	$\sigma_0 = 0.7\sigma_{TS}$ MPa	F_0 Hz
Tungsten	411	1920	19.2×10^3	4.5×10^{-6}	1344	6597
Stainless steel	190–210	460–860	7.96×10^3	$(16–18) \times 10^{-6}$	462	6023
Beryllium bronze	131	700	8.26×10^3	17.5×10^{-6}	490	6089

As the upper limit of the wire temperature range, in figure 10, we set the value as that corresponding to where the frequency drops to 1000 Hz, below which the autogeneration system typically does not provide a stable process of oscillation generation.

2.4 Frequency dependence on ambient temperature

VWMs are also affected by the ambient temperature. Let us consider that the wire is also exposed to a local heat source. For certainty, we introduce the following three temperatures:

$T_A(t)$ — ambient temperature,

$T_B(t)$ — temperature of the VWM base,

$T_W(t)$ — temperature of the VWM wire.

We assume that the ambient temperature variation is sufficiently gradual, so that

$$T_A(t) = T_B(t). \tag{2.8}$$

In addition, the temperature of the wire is divided into two components: the ambient temperature and the excess $T^{\mathrm{ag}}(t)$ over this temperature due to the local source that only affects the wire. Therefore,

$$T_W(t) = T_A(t) + T^{\mathrm{ag}}(t). \tag{2.9}$$

In fact, we neglect the low flow of heat from the wire to the clamps and base, noting their heat capacity difference and poor heat transfer by contact.

At the start of the experiment ($t = 0$),

$$T_A(0) = T_B(0) = T_W(0) = T_0, \tag{2.10}$$

where T_0 is the initial temperature, and at measuring time t,

$$F(t) = \frac{1}{L}\sqrt{(\sigma_{\mathrm{o}} + E_W(\alpha_B - \alpha_W)(T_A(t) - T_0) - E_W\alpha_W T^{\mathrm{ag}}(t))/\rho}. \tag{2.11}$$

As can be understood, the frequency response accumulates the signal of the wire temperature change and is also subject to the ambient temperature changes (in the case of a long-duration experiment, this will be perceived as a drift in the initial frequency).

The process of wire stretching when the ambient temperature changes in addition to the heating from the beam impact (local source) is schematically shown in figure 11.

One can see that in the specific case

$$\alpha_B - \alpha_W = 0, \tag{2.12}$$

the frequency does not depend on the ambient temperature. We call this type of sensor a temperature-compensated VWM. However, one should note that this compensation occurs only for very slow processes.

2.5 VWM with reference wire

An alternative approach is to manufacture a sensor with two vibrating wires: one is exposed to the beam, and the second one is used as reference for considering the gradual changes in the ambient temperature (see figure 12).

2021 JINST 16 R01001

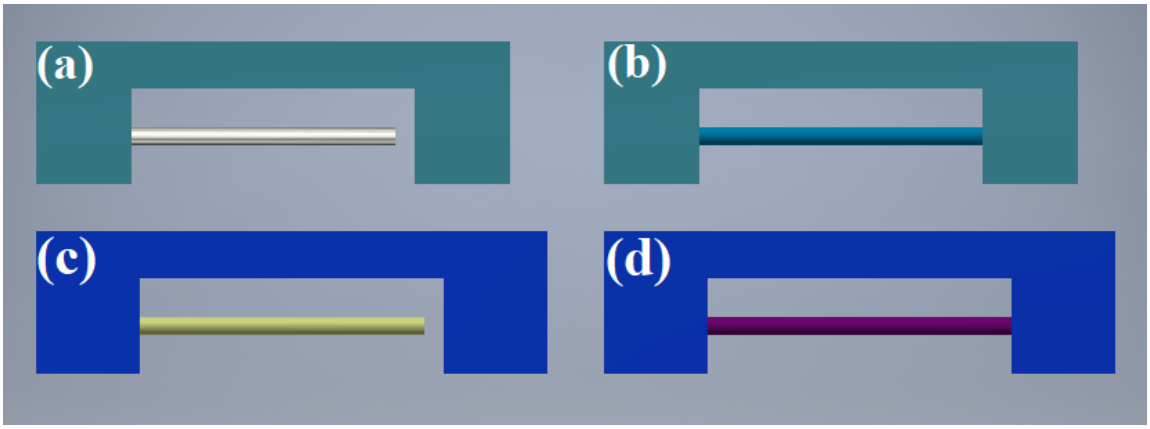

Figure 11. Tensioning wire when ambient temperature changes, as well as additional heating from beam impact. (a) Base (cadet blue) — length of bed for wire $L_B^0 = 30\,\text{mm}$, wire (silver) — length in non-tensioned state $L_W^0 = 28\,\text{mm}$. (b) Wire (sky blue medium) is stretched on bed length of base and becomes $L_B^0 = 30\,\text{mm}$, i.e., tension of wire is calculated using $\Delta L_W^0 = 2\,\text{mm}$. (c) Base (clear blue) — as ambient temperature changes, bed length becomes $L_B = L_B^0(1+\alpha_B\Delta T) = 32\,\text{mm}$, whereas wire (satin lemon chiffon) length in non-tensioned state increases to $L_W = L_W^0(1+\alpha_W\Delta T) = 29\,\text{mm}$, on heating. In addition, wire is also heated by additional source, i.e., measured beam. Thus, total length of non-tensioned wire becomes $L_W = L_W^0(1+\alpha_W(\Delta T+\Delta T^{\text{ag}})) = 30\,\text{mm}$. (d) Wire (smooth purple) is stretched along bed length of base and becomes 32 mm, i.e., wire tension is calculated using $\Delta L_W = 2\,\text{mm}$.

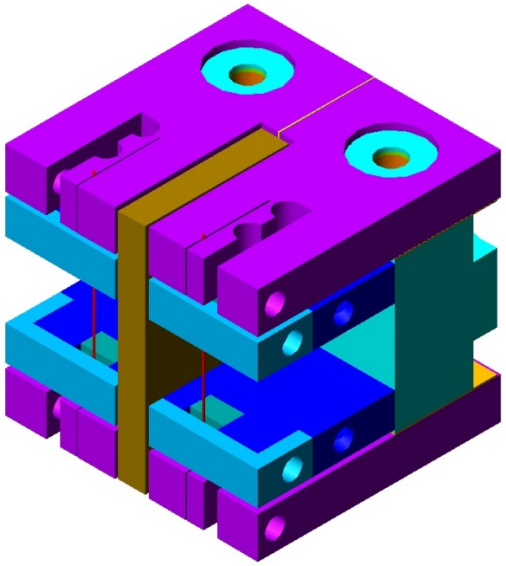

Figure 12. Double-wire vibrating wire monitor (DW-VWM).

In this case, the VWM consists of two identical wires on a common base. One wire (first, with temperature $T'_W(t)$) is exposed to the beam; the other (second, with temperature $T''_W(t)$) serves as a reference. For the second wire, we assume $T''_W(t) = T_A(t)$. As in the previous case, we divide the temperature of the first wire into two components: ambient temperature and the impact of a local

2021 JINST 16 R01001

source that acts only on the first wire. To determine this impact, we have two equations:

$$F'(t) = \frac{1}{L}\sqrt{(\sigma_o + E_W(\alpha_B - \alpha_W)(T_A(t) - T_0) - E_W\alpha_W T^{ag}(t))/\rho}, \tag{2.13}$$

$$F''(t) = \frac{1}{L}\sqrt{(\sigma_o + E_W(\alpha_B - \alpha_W)(T_A(t) - T_0))/\rho}. \tag{2.14}$$

From these equations, one can finally obtain

$$T^{ag}(t) = \frac{L^2\rho}{E_W\alpha_W}\left[\left((F''(t))^2 - (F_0'')^2\right) - \left((F'(t))^2 - (F_0')^2\right)\right]. \tag{2.15}$$

2.6 Thermal balance of VWM

The beam penetrating the wire loses some energy and heats the wire. The wire temperature increase relative to its initial temperature can be calculated by the equation of balance between the power deposited in the wire and the heat sink through all possible thermal mechanisms. These mechanisms are conduction along the wire to the end clips, convection losses to the ambient atmosphere (if air or another gas is present), and losses through the radiation to the ambient space. It is assumed that there are no other heat sources except the beam impact, and that the profile of the balanced temperature has a triangle profile along the wire (i.e., at the wire ends we set the temperature to T_0, and at the middle to the maximal temperature T_{MAX}). This approximation is sufficiently close to real temperature profile along the wire. The balance equation is written as

$$W_{beam} = W_\lambda + W_{rad} + W_{conv}, \tag{2.16}$$

where W_{beam} is the deposited power from the beam into the wire,

$$W_\lambda = 8\,(T - T_0)\,\lambda S/L \tag{2.17}$$

is the conductive heat sink,

$$W_{rad} = \varepsilon\sigma_{ST\_B}T_W^4\pi dL - \varepsilon\sigma_{ST\_B}T_0^4\pi dL \tag{2.18}$$

is the heat sink through the radiation (here, we consider temperature in Kelvin), and

$$W_{conv} = \delta\,(T_W - T_0)\,\alpha_{conv}\pi dL \tag{2.19}$$

is the convection heat sink. Eqs. (2.17)–(2.19) are obtained in assumption that thermal conductivity and the radiation coefficient are independent of temperature.

Here, T_0 is the ambient temperature, $T_{W,MEAN} = ((T_{MAX}+T_0)/2)$ is the wire mean temperature, d and L are the diameter and length of the wire, respectively, S is the wire cross-section, λ is the thermal conductivity of the wire material, σ_{ST_B} is the Stefan-Boltzmann constant, ε is the emissivity of the wire, α_{conv} is the convection heat transfer coefficient, $\delta = 1$ if the wire is placed in atmosphere, and $\delta = 0$ if the wire is placed in vacuum. Equations (2.17)–(2.19) are obtained with the assumption that the thermal conductivity and emissivity do not depend on temperature. This is a reasonable assumption for an order-of-magnitude estimate, because in the temperature range up to several hundred Celsius degrees these parameters are weakly dependent on temperature.

2021 JINST 16 R01001

Introducing parameter $\Delta T = (T_{\mathrm{W,MEAN}} - T_0)/2$ (denoting overheating of the wire), the following relation between ΔT and W_{beam}can be obtained:

$$\Delta T = \frac{W_{\mathrm{beam}}}{8\lambda S/L + 4\varepsilon\sigma_{ST\_B}T_0^3\pi dL + \delta\alpha_{\mathrm{conv}}\pi dL}. \tag{2.20}$$

For parameter α_{conv}, we use the equation for convection of a cylinder by air with speed ν, i.e.,

$$\alpha_{\mathrm{conv}} = 4.13\frac{\nu^{0.8}}{d^{0.2}}. \tag{2.21}$$

An important parameter of the VWM is its response time that represents the thermal inertia of the wire and it can be estimated as follows:

$$\tau = \frac{c\rho}{8(\lambda/L^2 + 2\varepsilon\sigma_{ST\_B}T_0^3/d + \alpha_{\mathrm{conv}}/2d)}, \tag{2.22}$$

In case of vacuum, the value of α_{conv} should be set to zero.

Thermal inertia of a wire imposes certain restrictions on the scanning speed of the beam. We have performed dedicated research on the effect of scanning speed on the measurement results of a semiconductor laser beam. Since the profile of such a beam was not known a priori, we took coincidence of scans in forward and backward directions as a criterion for adequacy of measurement results. The measurement results for a stainless steel wire (in air) are shown in figure 13 (see [39]).

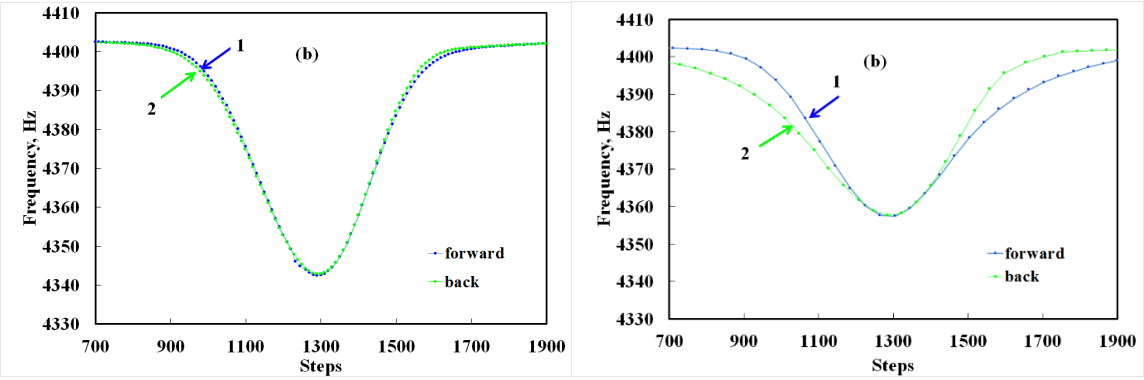

Figure 13. Forward and backward scans of VWM. Forward (backward) represents movement with increasing (decreasing) number of steps. (a) Scanning with speed of 50 steps/s (0.0830 mm/s). Curves 1 and 2 are forward (movement in the direction of increasing step) and backward scans, respectively. (b) Scanning with speed of 200 steps/s (0.3322 mm/s).

Comparative characteristics of forward and backward scans are presented in table 2.

Note that such preliminary measurements are desirable for other types of wire and measurement conditions (e.g., in vacuum or other atmosphere).

In table 3, we summarize the thermal parameters of a VWM with a tungsten wire. The VWM can operate in air or in vacuum. In the last column (i.e., total power loss in vacuum), the convection losses are not included.

One can see that the thermal losses by convection and thermal conductivity are in the same order, whereas the losses through the radiation become significant at overheating temperatures higher than 100 K.

2021 JINST 16 R01001

Table 2. Comparative characteristics of forward and backward beam scans at different speeds.

Speed, mm/s	Beam FWHM, mm	Beam FWHM scan time, s	Measurement numbers	Frequency drop, Hz	Coincidence of the scans, Hz	Profile measurement accuracy, %
0.0166	0.556	33.5	987	68	0.11	0.16
0.0332	0.553	16.6	492	63	0.20	0.32
0.0830	0.566	6.8	194	60	0.42	0.70
0.1661	0.602	3.6	97	51	1.03	2.01
0.2491	0.622	2.6	63	50	2.45	4.89
0.3322	0.715	2.1	48	45	3.22	7.15

Table 3. Thermal parameters of VWM with tungsten wire.

Wire temperature rise, K	Frequency, Hz	W_{conv}, W	W_{λ}, W	W_{rad},W	$W_{\text{total in air}}$, W	$W_{\text{total in vacuum}}$, W
0	6.51×10^3	0	0	0	0	0
0.001	6.51×10^3	2.14×10^{-7}	2.72×10^{-7}	5.02×10^{-8}	5.36×10^{-7}	3.22×10^{-7}
0.01	6.51×10^3	2.14×10^{-6}	2.72×10^{-6}	5.02×10^{-7}	5.36×10^{-6}	3.22×10^{-6}
0.1	6.51×10^3	2.14×10^{-5}	2.72×10^{-5}	5.02×10^{-6}	5.36×10^{-5}	3.22×10^{-5}
1	6.51×10^3	2.14×10^{-4}	2.72×10^{-4}	5.04×10^{-5}	5.36×10^{-4}	3.22×10^{-4}
10	6.47×10^3	2.14×10^{-3}	2.72×10^{-3}	5.28×10^{-4}	5.38×10^{-3}	3.25×10^{-3}
100	6.04×10^3	2.14×10^{-2}	2.72×10^{-2}	8.22×10^{-3}	5.68×10^{-2}	3.54×10^{-2}
200	5.52×10^3	4.27×10^{-2}	5.43×10^{-2}	2.58×10^{-2}	1.23×10^{-1}	8.01×10^{-2}
400	4.30×10^3	8.55×10^{-2}	1.09×10^{-1}	1.11×10^{-1}	3.06×10^{-1}	2.20×10^{-1}
600	2.55×10^3	1.28×10^{-1}	1.63×10^{-1}	3.14×10^{-1}	6.05×10^{-1}	4.77×10^{-1}

Table 4. Thermal parameters of VWM with stainless steel wire.

Wire temperature rise, K	Frequency, Hz	W_{conv}, W	W_{λ}, W	W_{rad}, W	$W_{\text{total in air}}$, W	$W_{\text{total in vacuum}}$, W
0	6.01×10^3	0	0	0	0	0
0.001	6.01×10^3	2.14×10^{-7}	2.67×10^{-8}	5.02×10^{-8}	2.91×10^{-7}	7.69×10^{-8}
0.01	6.01×10^3	2.14×10^{-6}	2.67×10^{-7}	5.02×10^{-7}	2.91×10^{-6}	7.69×10^{-7}
0.1	6.01×10^3	2.14×10^{-5}	2.67×10^{-6}	5.02×10^{-6}	2.91×10^{-5}	7.69×10^{-6}
1	5.99×10^3	2.14×10^{-4}	2.67×10^{-5}	5.04×10^{-5}	2.91×10^{-4}	7.71×10^{-5}
10	5.78×10^3	2.14×10^{-3}	2.67×10^{-4}	5.28×10^{-4}	2.93×10^{-3}	7.95×10^{-4}
100	3.07×10^3	2.14×10^{-2}	2.67×10^{-3}	8.22×10^{-3}	3.23×10^{-2}	1.09×10^{-2}

In table 4, we summarize the same thermal parameters as above of a VWM with a stainless steel wire.

Thermal characteristics of VWM sensors for wires made of different materials are given in table 5. Here, the wire length is 40 mm and the diameter is 0.1 mm.

It should be noted that we fully calculated the sensor response time, considering only the thermal processes occurring in the wire. In autogeneration boards, the feedback circuit uses a capacitor with different values, which affects the start time of the vibration generation. It was

2021 JINST 16 R01001

Table 5. Thermal characteristics of VWM.

	Frequency resolution Hz	Thermal resolution mK	Deposited power resolution (air), mkW	Deposited power resolution (vacuum), mkW	Response time (air) s	Response time (vacuum) s	Dynamic range
Stainless steel	0.01	0.3	0.007	1	20	0.23	7.1×10^5
Bronze	0.01	0.6	0.05	2.6	9	0.21	3.5×10^5
Tungsten	0.01	1	0.3	5.4	2	0.16	4.4×10^5

interesting to compare the performance of the monitor with two significantly different capacitor values when a heating source per wire is turned on abruptly. Heating was simulated by turning the laser light on/off on the wire. Recording the corresponding frequency change showed that the time characteristics of the monitor did not change (see figure 14).

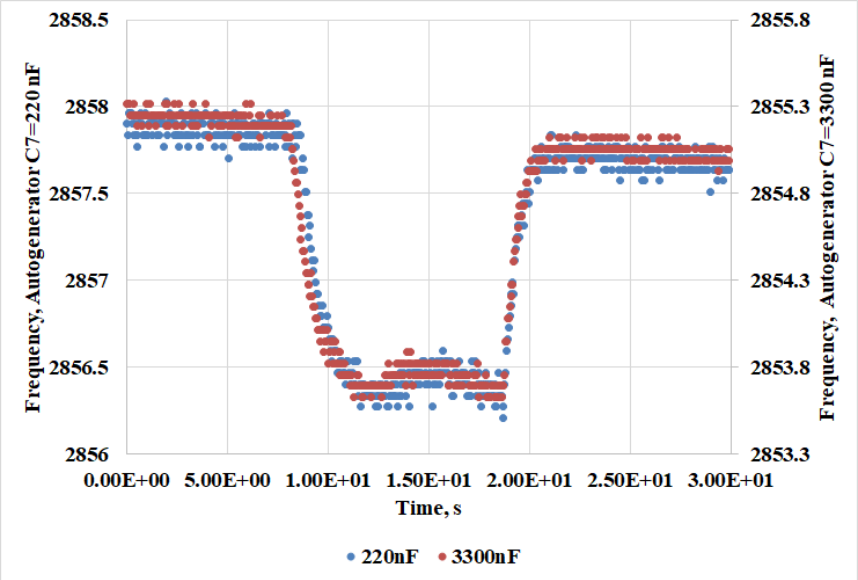

Figure 14. Response of vibrating wire monitor to abrupt on/off of heating source when using different capacitor C' values in autogeneration board. Blue line corresponds to $C = 220\,\text{nF}$ and brown line to $C = 3300\,\text{nF}$.

From the point of view of oscillation amplitude stabilization, $C = 3300\,\text{nF}$ value is preferable, although it increases the time of the autogeneration mode setting when the monitor power supply is switched on (compare figures 7 and 8).

3 Beam losses in matter

The most important parameter for a given configuration of measured particles and a VWM with a wire of a specific material is the energy that one particle loses when penetrating the wire (parameter W_{beam} in eq. (2.20)). The rule of energy loss calculations is strongly dependent on the type of particles.

2021 JINST 16 R01001

3.1 Protons/ions

For heavy particles (protons and ions), parameter W_{beam} in eq. (2.20) is determined by the ionization losses of the particles penetrating the wire material. The equation for specific ionization losses dE/dx of a particle with mass $M \gg m_e$ (m_e — electron mass) and velocity v is known as the Bethe-Bloch formula, which is the basic expression used for energy loss calculations [40],

$$-\frac{dE}{dx} = 2\pi N_A r_e^2 m_e c^2 \rho \frac{Z}{A}\frac{z^2}{\beta^2}\left[\ln\left(\frac{2m_e c^2\gamma^2\beta^2 W_{\max}}{\Phi^2}\right) - 2\beta^2 - \delta - 2\frac{C}{z}\right], \tag{3.1}$$

where $2\pi N_A r_e^2 m_e c^2 = 0.1535\times10^{-4}$ MeV·m^2/mol, $N_A = 6.022\times10^{23}$ mol^{-1} — Avogadro's number, $r_e = 2.817\times10^{-15}$ m is the classical electron radius, ρ is the density of the absorbing material in g/cm^3, Z is the atomic number of the absorbing material, z is the charge of the incident particle in units of electron charge, A is the atomic weight of the absorbing material in g/mol, Φ is the mean ionization potential in eV, $\beta = v/c$; $\gamma = 1/\sqrt{1-\beta^2}$, c is the speed of light, δ is the amendment that considers the effect of medium density, C is the correction effect of the binding of the electrons on K- and L-shells, and $W_{\max}$ is the maximum energy transfer in a single collision. The maximum energy transfer in the case of proton mass $m_p \gg m_e$ is $W_{\max} \approx 2m_e c^2\gamma^2\beta^2$. Equation (3.1) works well for protons and ions. For electrons and positrons, the Bethe—Bloch formula differs from eq. (3.1).

In table 6, some typical values for the proton ionization losses in tungsten ($Z = 74$, $A = 183.84$ g/mol, $\rho = 19.3$ g/cm^3) are presented without corrections in two proton energy ranges.

Table 6. Ionization losses dE_p/dx for proton in tungsten (E_p is proton kinetic energy).

E_p, MeV	dE_p/dx, MeV/cm	E_p, MeV	dE_p/dx, MeV/cm
10	384.63	1000	23.87
11	359.92	2000	22.63
12	338.57	3000	23.04
13	319.92	4000	23.66
14	303.46	5000	24.29
15	288.83	6000	24.88
16	275.73	7000	25.43
17	263.91	8000	25.92
18	253.20	9000	26.37
19	243.44	10000	26.79
20	234.50		
21	226.29		
22	218.71		
23	211.70		
24	205.18		
25	199.11		

For one proton, the energy loss, δ_p, in the wire can be approximated as

$$\delta_p = \left(\frac{dE_p}{dx}\right) \times (\pi d/4). \tag{3.2}$$

2021 JINST 16 R01001

Some of the proton energy losses will be transferred as heat in the wire material. The ratio of this energy transport, $\varepsilon_{\text{heat}} \approx 0.3$–$0.7$, depends on the proton energy, parameters of the wire material, and wire geometry. Typically for preliminary calculations, we set $\varepsilon_{\text{heat}} \approx 0.3$.

The equation that determines the frequency shift of the wire oscillation depends on the proton beam current, I_p, penetrating the wire as follows:

$$\frac{\Delta F}{F_0} = -\frac{E}{2\sigma_0} \frac{\alpha \varepsilon_{\text{heat}} (\delta_p I_p / e)}{\left[8\lambda S/L + 4\varepsilon\sigma_{ST\_B} T_0^3 \pi dL + \eta \alpha_{\text{conv}} \pi dL\right]}. \tag{3.3}$$

3.2 Electrons, positrons, muons, photons

Modified Bethe-Bloch formulae for ionization losses for electrons and positrons can be found in ref. [41]. To estimate the electron energy losses in matter, processes besides ionization should also be considered [10]: creation of electron-positron pairs, secondary electron emission (SEM, at low energy), emission of photons, elastic and inelastic scattering, dislocations, production of secondary particles (at high energy), Cherenkov radiation, bremsstrahlung radiation, and optical transition radiation (OTR). The corresponding data for electrons moving in lead are presented in [42].

A unique case is the interaction of muon beams with matter. Muon accelerator is an interesting type of accelerator that offers unique potential for particle physics applications. The concept of a muon collider was first proposed in 1969 [43]. A particular muon accelerator program (MAP) was initiated in 2010, aiming at developing the concepts and technologies required for muon colliders and neutrino factories [44]. An example of muon losses in copper due to various interaction processes can be found in [10].

The loss of photon beams in a material depends on the photon energy and the composition of the material. For energies of the photon (x-ray, gamma ray, bremsstrahlung) from 1 keV to 20 MeV, energy-absorption coefficients for elements Z = 1 to 92 and 48 additional substances of dosimetric interest are presented in [45].

4 VWM applications

VWMs are applicable in various configurations for different purposes. Below are the examples of such applications. Section 4.1 presents VWM applications for the accelerator beam diagnostics that have already been tested. Some of the results were reported in detail elsewhere. Section 4.2 presents new applications of the VWM for accelerator diagnostics. Proposals for the use of wires separated by a screen, and for composite wires to measure neutron beams are introduced based on our previous studies. A proposal for the use of the vibrating wire technology for measuring the impact of radiation (including neutrons) on the elastic properties of materials is newly made here. Non-thermal applications of vibrating wires are described in section 5.

4.1 VWMs already implemented for accelerator diagnostics

Electron beam scanners. Initial experiments on scanning charged particle beams were conducted on the electron beam of the synchrotron injector of Yerevan Physics Institute with energy 50 MeV and average current of approximately 10 nA after collimation [46] (see figure 15). A monitor with a large aperture formed by a 50-mm-long target wire was also used to measure the electron beam profile (see [30]).

2021 JINST 16 R01001

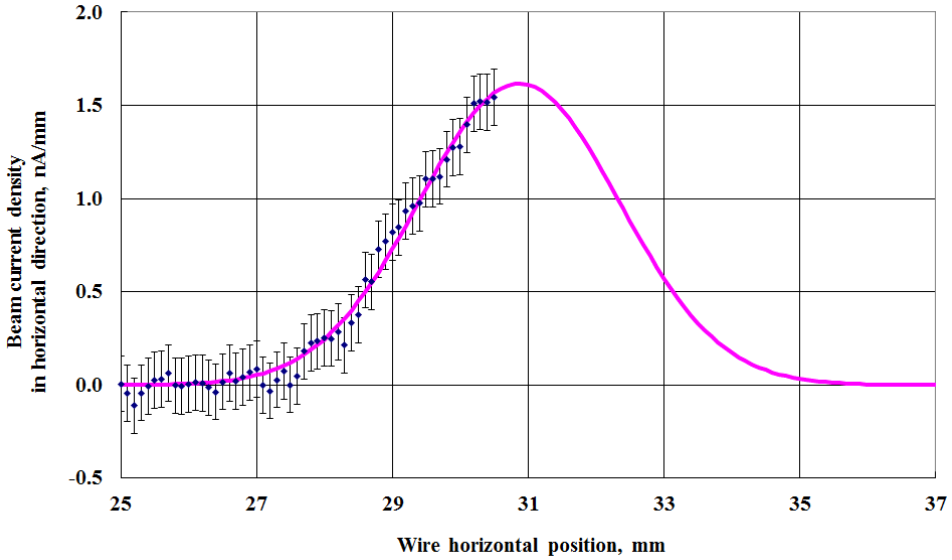

Figure 15. First experimental results of transverse profile measurements applying vibrating wire scanner on electron beam at Yerevan synchrotron injector. Horizontal profile of 6 nA beam was reconstructed from frequency scan. The beam feed system restricted the scanner movement only to the half of the beam. Nevertheless, this experiment showed for the first time the response of the vibrating wire to a sufficiently small current of the electron beam.

Proton beam scanners. A series of experiments on the use of a VWM on a proton beam was conducted at the PETRA accelerator at DESY, where PETRA serves as a proton booster for HERA. The unique characteristics of the VWM allowed measuring the halo region of the proton beam with an average current of approximately 15 mA and energy of 15 GeV [47–50] (see figure 16). From figure 16(b) one can see that frequency response on wire position is started at immediately at movement from parking position (Pos = 0 mm), while the photomultiplier signal begins to form at a much greater depth of scanning (Pos = 14 mm).

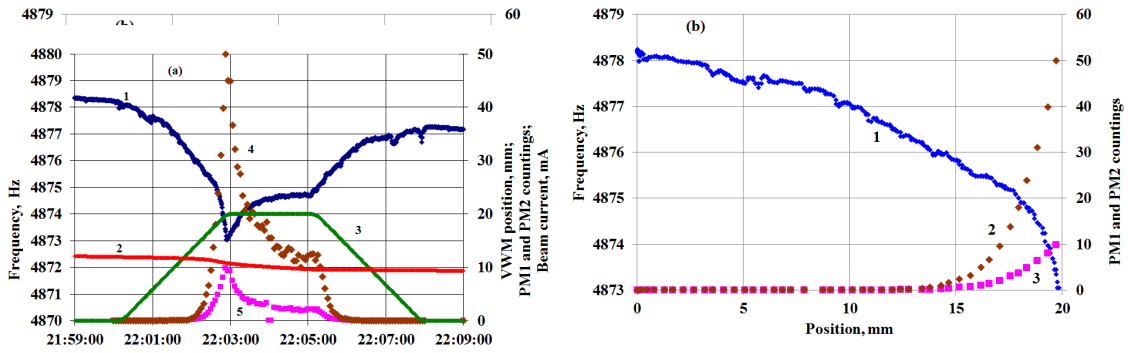

Figure 16. PETRA (DESY) proton beam scan by VWM: (a) time dependence, 1 — frequency signal, 2 — proton beam current, 3 — scan depth, 4, 5 — responses of photomultipliers, (b) position dependence, 1 — frequency signal, 2, 3 — responses of photomultipliers

2021 JINST 16 R01001

A monitor with an expanded aperture of 60 mm and a total wire length of 120 mm was installed on the transport line between the linear accelerator and the 3-GeV synchrotron of the J-PARC complex. The ability of the monitor to diagnose a beam halo was confirmed. As a positive characteristic, it was noted that the sensor was insensitive to secondary electrons [51].

The extended aperture of the VWM was planned to be used to study the proton beam halo in the Project-X Injector Experiment (PXIE, Fermilab), which was an R&D program for developing a multi-megawatt superconducting proton accelerator. The VWM was tested on a Fermilab high-intensity neutrino source (HINS) set-up with a 50-keV proton beam [31, 32].

Proton beam profiling in air by a VWM was conducted at the Korea Multi-purpose Accelerator Complex (KOMAC) facility under low (100 nA) beam-current conditions [25, 52].

Ion beam scanners. A VWM was tested on a beam of iron ions with energy of 20 keV and a current of 16 pA of the EMAL-2 energy-mass analyzer. A frequency shift at a level of 0.15 Hz was obtained (see [50]).

Laser beam scanners. Generally laser beams, as the most accessible heat sources for experiments, are used in the process of developing and calibrating all types of VWMs. Specifically, conventional semiconductor lasers with a power from a few to several hundred mW are used. The laser beam profiling itself, however, may be an independent research topic of interest [53]

X-ray (undulator) radiation scanners. Although X-ray radiation only deposits a small part of its energy in the wire, owing to the high sensitivity of VWMs, this energy is sufficient to heat the vibrating wire at the level of the frequency shift resolution. Experiments were performed at the APS-ANL to measure the X-ray profile from an undulator with an energy range of 6.5–19.5 keV and an unfocused beam of size 3 mm × 1.5 mm. An important task in this experiment was to measure the radiation only from the undulator, with suppression of the background by the softer synchrotron radiation photons generated when the electrons pass the magnetic fields of the focusing and deflecting magnets. This suppression was achieved by a beryllium filter plate. Consequently, only the X-ray emission of the undulator remained after the filter, which was measured by the VWM [33]. Experiments with two vertically-offset horizontal stainless steel wires for temperature diagnostics were conducted at APS beamline 19-ID (flux details: 1×10^{13} X-ray photons/s/mm^2, wavelength range 2.032–0.670 Å, energy range 6.1–18.5 keV, focused beam size 83 µm × 38 µm, and unfocused beam size 2.4 mm × 1.2 mm [54])

Owing to the high sensitivity of this technique, the studies were performed at extremely low power levels using the radiation from a 3.3-cm-period permanent magnet hybrid undulator with a 5-mA electron beam at an energy of 7 GeV. The X-ray beam was filtered by transmission through 7 mm of beryllium placed in the photon beam path, ensuring that only hard X-rays were detected. The VWM was installed in the vacuum chamber of the beamline with the vacuum level decreased to 10^{-9} Torr [55]. Results of the undulator X-ray beam measurements are presented in figure 17.

Synchrotron radiation scanners. At the APS-ANL synchrotron, an experiment was conducted to measure the parameters of the electron beam using the synchrotron radiation (SR). It is important that such a measurement is conducted outside the vacuum chamber behind the copper flange of one of the unused SR channels. In general, radiation with a power of approximately 99.1 W and a peak

2021 JINST 16 R01001

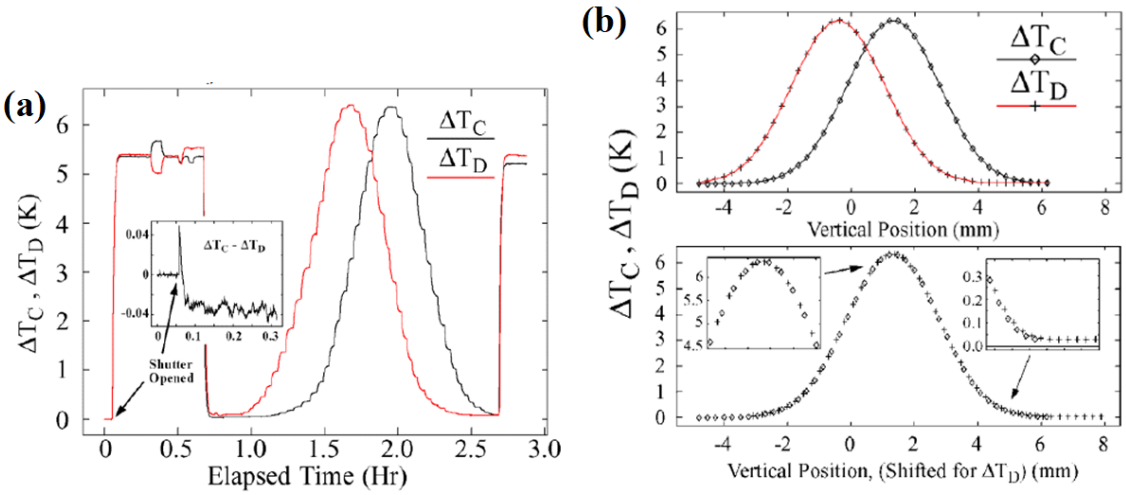

Figure 17. Undulator X-ray beam measurement by two-wire VWM at APS-ANL. (a) Data collected during vertical angle scan. (b) VWM data corrected for thermal drift and beam current decay. Two data sets are overlapped by introducing some offset in lower panel for direct comparison [33].

energy of approximately 10 keV was absorbed by a 6-mm-thick copper flange, and only hard X-ray photons with an energy of more than 100 keV (SR spectrum tail) with a power of 420 mW passed through the flange. Approximately 1.1 mW of the power was converted into heat and deposited on the wire. The electron beam of the synchrotron, using the magnetic optics of the accelerator, was scanned in an angle within the limits of 300 µrad with a step of 2.4 µrad. A special five-wire monitor was developed. Profile of the synchrotron radiation was obtained in the vertical direction in air [34]. A picture of the VWM and the profiling results are presented in figure 18.

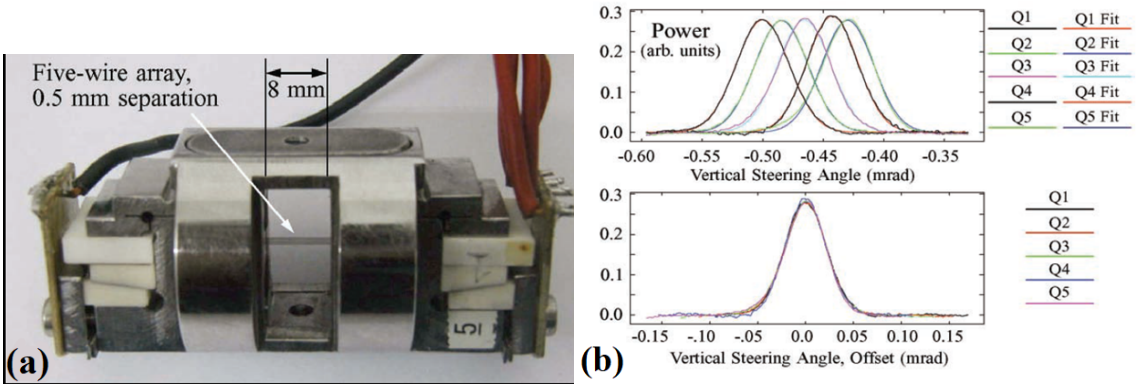

Figure 18. Synchrotron radiation vertical profile measurements by five-wire VWM at APS-ANL. (a) Monitor details. (b) APS bending magnet radiation power density profiles inferred from the VWM data. Top: measured profiles together with Gaussian fits. Bottom: the same measured data, shifted along the horizontal axis.

In [56], the mutual thermal influence of the wires on each other was considered and included when determining the profile.

2021 JINST 16 R01001

Large-aperture monitors. Monitors with a large aperture size are of interest for profiling large proton beams (up to 80 mm). Two types of such monitors are developed:

- Direct action of the beam on a vibrating wire: a distinct scheme of the shock excitation of the process of autogeneration of oscillations is added to the electronic circuit [30, 57].
- Yoke type with two mechanically connected wires: a non-vibrating target wire of increased length that is exposed by the beam, and a vibrating wire measuring the change in the tension of the target wire are used together.

A yoke-type VWM with the length of the target wire, 60 mm, is presented in figure 19. Measurement of the temperature/tension of the target wire was performed using a special link between the two wires. The aperture of such monitors can reach 80 mm [31, 32]. The obtained data, including the beam test results at the HINS facility, indicate that the large-aperture VWM could be a useful diagnostic instrument in numerous present and future accelerators and be particularly effective for transverse beam halo measurements.

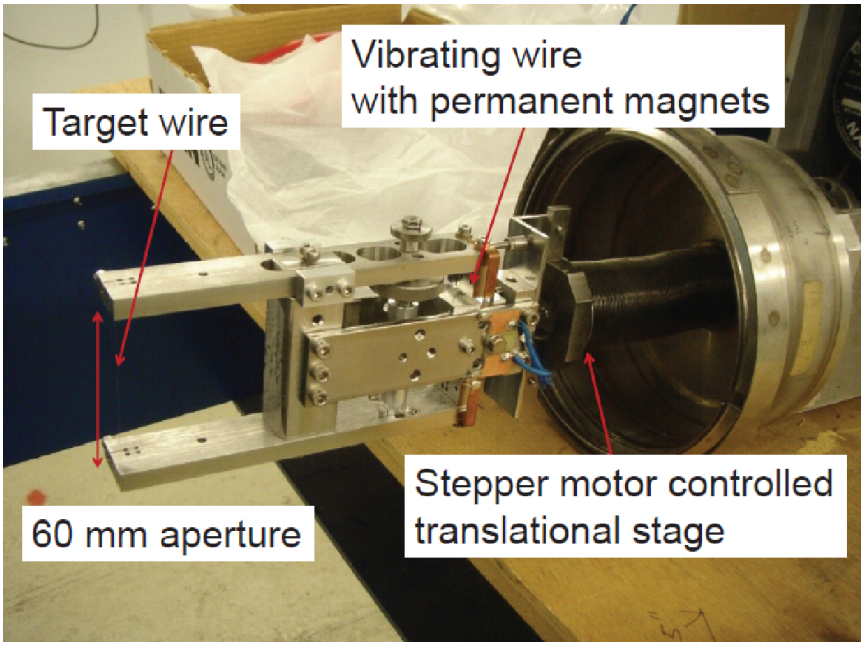

Figure 19. Large-aperture yoke-type vibrating wire monitor assembly. Two mechanically connected wires: target wire of 60 mm length exposed to the beam and a vibrating wire for sensing the tension of the target wire.

4.2 New proposals for VWM applications based on thermal method

Double-wire beam position monitors. Monitors with two wires spaced a few millimeters apart allow a differential method to control the beam shift between the wires. The method of differentiation of the signals of two wires can also be used to normalize monitors considering the influence of ambient temperature and the presence of other backgrounds besides the direct impact of the measured beam (one of the two wires is exposed to the beam, whereas the other wire is protected from the beam by a special screen and provides a reference signal). In [58], a type of double-wire

2021 JINST 16 R01001

monitor with an aperture increased by 8 mm is presented. This modification has a shorter response time and can be used both in vacuum and air.

A novel double-wire vibrating wire monitor (DW-VWM) consists of two wires spaced by a screen. Such a monitor is being developed for high-intensity accelerators, such as the joint European-Japanese project, IFMIF, specifically for the linear IFMIF prototype accelerator (LIPAc) (for details see [59]). The specific feature here is the high accelerator current (approximately 125 mA of the average beam current), which dictates the need for precise measurement of the flux of the lost particles and the halo region of the beam.

VWM with multilayer (composite) wires. A proposal on unique type of VWM with wires covered by a gadolinium layer was made for thermal neutron beam profiling [23]. Two unique properties are combined here: the unprecedented sensitivity of the natural frequency of a clamped vibrating wire to the wire temperature, and the remarkable ability of some gadolinium isotopes for neutron capture. ^{157}Gd has the highest thermal neutron capture cross-section among all the stable isotopes in the periodic table. We propose to measure the temperature increase in the wire containing gadolinium isotopes, which occurs when neutrons penetrate the wire and deposit some energy into the wire. We developed two types of VWMs for neutrons: small-scale with an approximately 10-µm-diameter tungsten wire and approximately 2-µm-thick Gd layer, and middle-scale with approximately 100-µm-diameter tungsten wire and an approximately 10-µm-thick Gd layer. For the first type, we offer to employ ^{157}Gd, which allows capturing all the thermal neutrons falling on the wire. For the second type, it is possible to use natural Gd.

VWM for elastic properties investigation. VMWs can also be useful for studying the effects of neutron fluxes on the elastic properties of the vibrating wire material. It is known that neutron fluxes when passing through a substance can affect its parameters, in particular, the mechanical properties of metals. The change in the mechanical properties of metals is caused by both neutron capture (mainly for neutrons with energy less than 1 MeV) and lattice disturbance during the atom-neutron collisions with energy more than 1 MeV. One of the mechanical parameters subject to changes under neutron irradiation is the elastic property of metals. In particular, there is noteworthy embrittlement of the materials, which reduces the lifetimes of the structures and assemblies in which these materials are used. It is proposed to use a vibrating wire exposed in the neutron flux, to observe the effect of neutron irradiation impact on the elastic properties of metals. The change in the elastic properties of the wire will be reflected in the values of the natural oscillation frequency of the wire and recorded accordingly. To determine the effect of the influence of a neutron flux on the oscillation frequency of the wire, it is proposed to use overstressed resonators, in which the wire is stretched by a tension comparable to the tensile limit of the materials (we typically used resonators in which the wire tension was less than this limit). It is suggested that a differential measurement scheme be used to compensate thermal and creep-related drifts of an overstressed material. A two-wire monitor, in which two wires are located in the same thermal space and are separated by a screen that significantly differentiates the exposure of neutrons to the wires, appears adequate to the task. The proposed method will allow characterizing the effects of neutron fluxes by comparison of the changes in the frequencies of both the wires.

2021 JINST 16 R01001

5 Other methods of using vibrating wire sensors

The proposals below concern the use of vibrating wires as a resonant target as well as for measuring thin beams. These proposals may be of great interest for accelerator diagnostics, however, at the moment they have been tested only on semiconductor laser beams and these preliminary results have been reported elsewhere (see refs. [60–64]).

5.1 Vibrating wire as resonance target

Recently, a new type of wire scanner for beam profile measurements was developed based on the use of a vibrating wire as a scattering target. Synchronous measurements with wire oscillations allow detecting only the signal originating from the scattering of the beam on the wire. This resonant method enables fast beam profiling in the presence of a high level of background. The concept was suggested in [60], and for photon beams it was realized in [61]. The method can be applied to different types of beams by simply choosing an appropriate detector for each case. For photon beams, fast photodiodes can be used, and for charged particles, scintillators combined with photomultipliers etc. are used.

The results of laser beam scans in a dedicated arrangement of laser and photodiode positions in which the photodiode registers two very similar peaks of different origins (one is caused by reflections from the vibrating wire and the other from the holder of the monitor) are presented in figure 20.

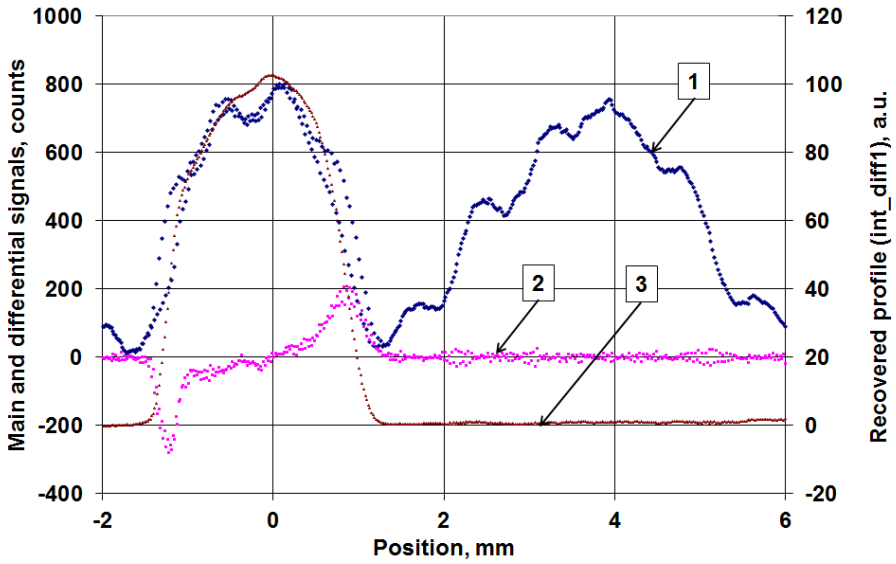

Figure 20. Vibrating wire as resonance target: photodiode measures reflections from both the vibrating wire and other mechanical parts of the resonant-type vibrating wire sensor (1, blue curve). Only the first type of the photodiode signal contributes to the differential signal (2, magenta curve). The algorithm developed in this study recovers the laser beam profile (3, brown curve).

In this experiment, the speed of the scanning does not exceed the speed of the wire during oscillations; however, even in this case, the time of full scanning can be reduced to approximately 100 ms. In [62], it is theoretically proved that the method can be applied using comparatively much

2021 JINST 16 R01001

higher scanning speeds. The increase in the scanning speed allows the method to be applied for the tomography of beams, i.e., for restoring a 2D profile of a beam by a set of one-dimensional scans performed at different angles in the transverse plane of the beam. The first attempt to use a VWM for laser beam tomography was tested in [63].

5.2 Vibration wire as miniature scanner for thin beam profiling

The measurement of beams of micrometer sizes is an important task in accelerator physics. A method for the profile measurements of small transverse size beams using a vibrating wire was proposed in [61, 64]. The main concept is to use the vibrating wire motion during its oscillations as the scanning mechanism and to synchronously measure the scattered/reflected particles/photons created by the interactions of the measured beam with the wire. The method is expected to be applicable to thin beams in particle accelerators. First, experimental results of a focused laser beam scanning were obtained in [64]. The concept was based on the measurement of reflected photons of a laser beam from the wire. The proof-of-principle test results, obtained using a laser beam including data processing and absolute calibration of the beam profile, as well as evaluation of the signal to noise ratio of the method, are presented in [36]. The schematic of the beam and vibrating wire interaction as well as obtained profile of the laser are presented in figure 21. Positioning of vibrating wire in both the precisely measured locations allows calibrating the profile in absolute coordinates. Further research will continue in this direction.

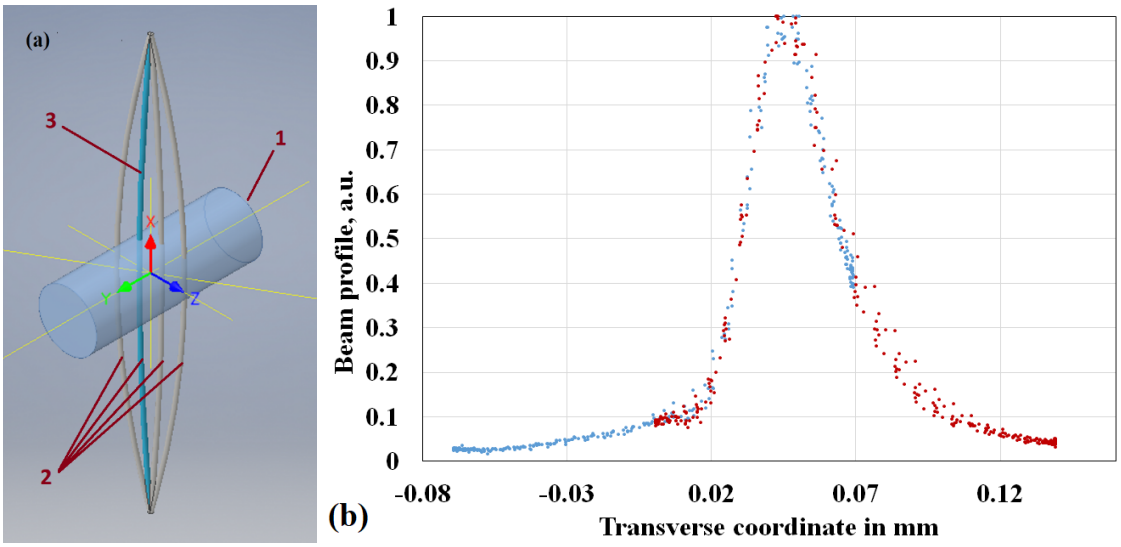

Figure 21. Schematic of beam and vibrating wire interaction and obtained profile. (a) Beam 1 is intercepted by an oscillating wire. X-axis is directed along the wire at its central position, y-axis is directed along the beam propagation, and z-axis is directed along the beam transverse direction. The positions of the wire at different times during its oscillation are denoted by 2 and 3. (b) Profile of the laser beam in absolute units (mm). Profile is recovered by measurements when the VWM in two positions shifts by 0.07 mm, which allows us to reconstruct the profile in absolute coordinates. Blue dots — profile recovered from measurement at the VWM position of 0.04 mm, orange dots — profile recovered from measurement at the VWM position of 0.11 mm.

2021 JINST 16 R01001

6 Conclusion

The thermal principle of VWMs enables measuring any type of beam that deposits a fraction of its energy in the wire. A wide dynamic range (in the temperature equivalent to fractions of milli Kelvin to hundreds of degrees), high accuracy of the measurements, good long-term stability, resistance to high background radiation and electromagnetic interference, and digital nature of the measurement of the output value (i.e., the frequency of natural oscillations of the wires) make this method a versatile tool for measuring the profiles of beams of charged particles, electromagnetic radiation, and neutrons in a wide range of energies. The large dynamic range, in particular, allows for measurements in both the halo and core of the beam.

It appears that the proposal to use a vibrating wire as the resonance target may also be of interest to accelerator diagnostics, as it allows detecting a well-defined frequency signal from the vibrating wire against the background of numerous particles and electromagnetic radiation unrelated to the beam scattering on the wire.

The proposal to use the motion of the oscillating wire as a scanner opens the opportunity for fast measurement of the profile of thin beams. With further improvement, this method can be developed to a tomographic method for the reconstruction of the two-dimensional profile of a beam. The method is promising both for accelerator diagnostics and for wider use of micron-sized beams.

Acknowledgments

We dedicate this article to the memory of J. Bergoz who had continuously supported and encouraged the activities on the vibrating wire monitors. We also miss I.E. Vasiniuk and M.R. Mailian for their fundamental contributions.

The authors would like to thank R. Reetz, N.M. Dobrovolski, I.G. Sinenko, S.L. Egiazaryan, K. Wittenburg, A.E. Avetisyan, A.E. Soghoyan, K.G. Bakshetyan, M.A Aginian., V.A. Oganessian, L.A. Poghosyan, G. Decker, G. Rosenbaum, J. Alonso, M.M. Davtyan, and D. Choe for their excellent and continuous collaboration on the subject of vibrating wires and their applications.

This research was supported by RA MES SCS in the frame of project 18T-1C031. This study was also supported by the National Research Foundation (NRF) of Korea (Grant Nos. NRF-2019R1F1A1062377 and NRF-2020R1A2C1010835).

References

[1] P. Forck, *Lecture Notes on Beam Instrumentation and Diagnostics*, Joint University Accelerator School, Gesellschaft fur Schwerionenforschung (GSI) Darmstadt, Germany, January–March 2011 [http://www.hep.ph.ic.ac.uk/fets/pepperpot/docs+papers/Fork_BeamInst_JUAS06.pdf].

[2] R. Jung, G. Ferioli and S. Hutchins, *Single pass optical profile monitoring*, in *Proceedings of the European workshop on beam diagnostics and instrumentation for particle accelerators*, 5–7 May 2003, Mainz, Germany, pp. 10–14;

[3] P. Forck et al., *Scintillation Screen Investigations for High Energy Heavy Ion Beams at GSI*, in *Proceedings of the European workshop on beam diagnostics and instrumentation for particle accelerators*, 16–18 May 2011, Hamburg, Germany, pp. 170–173

2021 JINST 16 R01001

[4] https://www.crytur.cz/products/scintillation-screens.

[5] G. Kube, *Particle beam diagnostics and control*, https://bib-pubdb1.desy.de/record/91024/files/KubeLecture.pdf.

[6] E.J. Jaeschke, S. Khan, J.R. Schneider and J.B. Hastings, *Synchrotron Light Sources and Free-Electron Lasers, Accelerator Physics, Instrumentation and Science Applications*, Springer International Publishing, Switzerland (2016).

[7] K. Manukyan, G. Zanyan, B. Grigoryan, A. Sargsyan, V. Sahakyan and G. Amatuni, *Beam Diagnostics for Areal Rf Photogun Linac*, in *Proceedings of the International Beam Instrumentation Conference*, 1–4 October Tsukuba, Japan, pp. 212–214.

[8] A. Murokh, J. Rosenzeig, V. Yakimenko, E. Johnson and X.J. Wang, *Limitations on the resolution of YAG:Ce beam profilemonitor for high brightness electron beam*, in *The Physics of High Brightness Beams*, World Scientific (2000), pp. 564–580.

[9] H. Koziol, *Beam diagnostics for accelerators*, CERN, Geneva, Swizterland (2001), https://cds.cern.ch/record/499098/files/p154.pdf.

[10] E. Bravin, *Transverse Beam Profiles*, in *Proceedings of the CERN Accelerator School on Beam Diagnostics*, 28 May – 6 June 2008, Dourdan, France, pp. 377–406

[11] K. Wittenburg, *Specific instrumentation and diagnostics for high-intensity hadron beams*, in *CERN Accelerator School on High Power Hadron Machines*, 28 March 2013, pp. 251–308 [arXiv:1303.6767].

[12] P. Strehl, *Beam Instrumentation and Diagnostics*, Springer-Verlag, Berlin, Heidelberg (2006).

[13] K. Wittenburg, *Beam size measurements using Wire Scanners at Synchrotron Light Sources and FELs or Wire scanners for Electron Beams (excluding Hadron Beams)*, http://bib-pubdb1.desy.de/record/403403/files/Wire%20Scanner%20Presentation.pdf.

[14] D.M. Harryman and C.C. Wilcox, *An upgraded scanning wire beam profile monitoring System for the ISIS high energy drift space*, in *Proceedings of the 6th International Beam Instrumentation Conference*, 20–24 August 2017, Grand Rapids, MI, U.S.A., pp. 396–400.

[15] S. Burger, C. Carli, M. Ludwig, K Priestnall and U. Raich, *The PS booster fast wire scanner*, in *Proceedings of the European workshop on beam diagnostics and instrumentation for particle accelerators*, 5–7 May 2003, Mainz, Germany, pp. 122–124.

[16] P. Dirksen, M. Lenckowski, W.R. Rawnsley, M. Rowe and V. Verzilov, *A Fast Wire Scanner for the TRIUMF Electron Linac*, in *Proceedings of the 6th International Beam Instrumentation Conference*, 20–24 August 2017, Grand Rapids, MI, U.S.A., pp. 401–403.

[17] M. Veronese et al., *A nanofabricated wirescanner: design, fabrication and experimental results*, in *Proceedings of the 6th International Beam Instrumentation Conference*, 20–24 August 2017, Grand Rapids, MI, U.S.A.,, pp. 314–317.

[18] S. Borrelli et al., *Wire Scanner on a Chip*, talk given at the *6th International Beam Instrumentation Conference*, 20–24 August 2017, Grand Rapids, MI, U.S.A., http://accelconf.web.cern.ch/AccelConf/ibic2017/talks/we2ab2_talk.pdf.

[19] X.J. Wang, I. Ben-Zvi, J. Sheehan and V. Yakimenko, *Brookhaven accelerator test facility energy upgrade*, in *Proceedings of the 1999 Particle Accelerator Conference*, 27 March – 2 April 1999, New York, NY, U.S.A., pp. 3495–3497.

2021 JINST 16 R01001

[20] A. Lumpkin, B. Yang, W. Berg, M. White, J. Lewellen and S. Milton, *Optical techniques for electron-beam characterizations on the APS SASE FEL project*, *Nucl. Instrum. Meth. A* **429** (1999) 336.

[21] S.G. Arutunian, N.M. Dobrovolski, M.R. Mailian, I.G. Sinenko and I.E. Vasiniuk, *Vibrating wire for beam profile scanning*, *Phys. Rev. ST Accel. Beams* **2** (1999) 122801 [physics/9901046].

[22] S.G. Arutunian, *Vibrating wire sensors for beam instrumentation*, in *Proceedings of the Beam Instrumentation Workshop*, 4–8 May 2008, Lake Tahoe, U.S.A., pp. 1–7 [MOSTFA01].

[23] S.G. Arutunian, J. Bergoz, M. Chung, G.S. Harutyunyan and E.G. Lazareva, *Thermal neutron flux monitors based on vibrating wire*, *Nucl. Instrum. Meth. A* **797** (2015) 37 [arXiv:1502.04050].

[24] F. Bourquin and M. Joly, *A magnet-based vibrating wire sensor: design and simulation*, *Smart Mat. Struct.* **14** (2004) 247.

[25] M.A. Aginian, S.G. Arutunian, D. Choe, M. Chung, G.S. Harutyunyan, S.Y. Kim et al., *Precise out-vacuum proton beam monitoring system based on vibrating wire*, *J. Cont. Phys.* **52** (2017) 110 [*Erratum ibid.* **52** (2017) 303].

[26] A.A.H. Pádua, J.M.N.A. Fareleira, J.C.G. Calado and W.A. Wakeham, *Electromechanical model for vibrating-wire instruments*, *Rev. Sci. Instrum.* **69** (1998) 2392.

[27] P.L. Woodfield and A.D. Seagar, *Viscous Drag Force and Heat Transfer from an Oscillating Micro-Wire*, in *Proceedings of the 18th Australasian Fluid Mechanics Conference*, 3–7 December 2012, Launceston, Australia

[28] J.T. Tough, W.D. McCormick and J.G. Dash, *Vibrating wire viscometer*, *Rev. Sci. Instrum.* **35** (1964) 1345.

[29] L. Bruschi and M. Santini, *Vibrating wire viscometer*, *Rev. Sci. Instrum.* **46** (1975) 1560.

[30] A.E. Avetisyan, S.G. Arutunian, I.E. Vasiniuk and M.M. Davtyan, *Yerevan synchrotron injector electron beam transversal scan with vibrating wire scanner*, *J. Cont. Phys.* **46** (2011) 247.

[31] S.G. Arutunian, A.E. Avetisyan, M.M. Davtyan, G.S. Harutyunyan, I.E. Vasiniuk, M. Chung et al., *Large aperture vibrating wire monitor with two mechanically coupled wires for beam halo measurements*, *Phys. Rev. ST Accel. Beams* **17** (2014) 032802.

[32] M. Chung et al., *Transverse beam halo measurements at high intensity neutrino source (hins) using vibrating wire method*, in *Proceedings of the International Particle Accelerator Conference*, 12–17 May 2013, Shanghai, China, pp. 819–821.

[33] G. Decker, S. Arutunian, M. Mailian and G. Rosenbaum, *First vibrating wire monitor measurements of a hard x-ray undulator beam at the Advanced Photon Source*, in *Proceedings of the European workshop on beam diagnostics and instrumentation for particle accelerators*, 20–23 May 2007, Venice, Italy, pp. 36–38.

[34] G. Decker, S. Arutunian, M. Mailian and I. Vasiniuk, *Hard X-ray synchrotron measurements at the APS with vibrating wire monitor*, in *Proceedings of the Beam Instrumentation Workshop*, 4–8 May 2008, Lake Tahoe, U.S.A., pp. 36–40.

[35] E.G. Lazareva, *Vibrating wire for profile measurements of thin beams in particle accelerators: Preliminary tests using a laser beam*, *J. Cont. Phys.* **53** (2018) 136.

[36] S.G. Arutunian, S.A. Badalyan, M. Chung, E.G. Lazareva, A.V. Margaryan and G.S. Harutyunyan, *A method for profile measurements of small transverse size beams by means of a vibrating wire*, *Rev. Sci. Instrum.* **90** (2019) 073302.

2021 JINST 16 R01001

[37] https://www.goodfellow.com/.

[38] http://www.matweb.com/search/datasheet.aspx?matguid=ff8cccd594eb46afbe82d15bf06e.

[39] S.G. Arutunian, G.S. Harutynyan, D. Choe, M. Chung, E.G. Lazareva and A.V. Margaryan, *Effects of scanning speed on the laser beam profile measurements by vibrating wire*, *J. Cont. Phys.* **52** (2017) 366.

[40] W.R. Leo, *Techniques for Nuclear and Particle Physics Experiments*, Springer-Verlag, New York, Berlin, Heidelberg (1987).

[41] I. Wingerter-Seez, *Particle Physics Instrumentation*, in *2nd Asia-Europe-Pacific School of High-Energy Physics*, pp. 295–314, 2017, DOI [arXiv:1804.11246].

[42] K.A. Olive, *Review of Particle Physics*, *Chin. Phys. C* **38** (2014) 090001 [update 2005].

[43] G.I. Budker, *Accelerators and colliding beams*, in *Proceedings 7th International Conference High-Energy Accelelerators*, 27 August – 2 September 1969, Yerevan, USSR, *Conf. Proc. C* **690827** (1969) 33.

[44] M.A. Palmer et al., *Muon accelerators for the next generation of high energy physics experiments*, in *Proceedings of the International Particle Accelerator Conference*, 12–17 May 2013, Shanghai, China, pp. 1475–1477.

[45] J.H. Hubbell and S.M. Seltzer, *X-Ray Mass Attenuation Coefficients*, *NIST Standard Reference Database 126* (2004).

[46] S.G. Arutunian, N.M. Dobrovolsky, M.R. Mailian and I.E. Vasinyuk, *Vibrating wire scanner: First experimental results on the injector beam of the Yerevan synchrotron*, *Phys. Rev. ST Accel. Beams* **6** (2003) 042801.

[47] S.G. Arutunian, M.R. Mailian and K. Wittenburg, *Vibrating wires for beam diagnostics*, *Nucl. Instrum. Meth. A* **572** (2007) 1022.

[48] S.G. Arutunian, M. Werner and K. Wittenburg, *Beam tail measurements by wire scanners at DESY*, in *ICFA Advanced Beam Dynamic Workshop: Proceedings of Beam HALO Dynamics, Diagnostics, and Collimation (in conjunction with 3rd workshop on Beam-beam Interaction)*, May 19–23 2003, Gurney's Inn, Montauk, NY, U.S.A., *AIP Conf. Proc.* **693** (2003) 129.

[49] S.G. Arutunian et al., *Problems of Installation of Vibrating Wire Scanners into Accelerator Vacuum Chamber*, in *Proceedings of the 8th European Particle Accelerators Conference*, 3–7 June 2002, Paris, France, pp. 1837–1839.

[50] S.G. Arutunian et al., *Vibrating wire scanner parameters optimization*, in *Proceedings of the 9th European Particle Accelerators Conference*, 5–9 July 2004, Lucerne, Switzerland, pp. 2457–2459

[51] K. Okabe, M. Yoshimoto, K. Yamamoto and M. Kinsho, *A preliminary study of the vibration wire monitor for beam halo diagnostic in J-PARC L3BT*, in *Proceedings of the International Particle Accelerator Conference*, 12–17 May 2013, Shanghai, China, pp. 535–537.

[52] D. Choe, M. Chung, S.Y. Kim, S.G. Arutunian, A.V. Margaryan and E.G. Lazareva, *Beam Halo Measurements using Vibrating Wire at the KOMAC*, in *Proceedings of the International Particle Accelerator Conference*, 8–13 May 2016, Busan, Korea, pp. 680–682.

[53] M.A. Aginian, S.G. Arutunian, V.A. Hovhannisyan, M.R. Mailian and K. Wittenburg, *Vibrating wire scanner/monitor for photon beams with wide range of spectrum and intensity*, in *Proceedings of the NATO Advanced Research Workshop "Advanced Photon Sources and Their Application"*, 29 August – 2 September 2004, Nor Amberd, Armenia, pp. 335–342.

2021 JINST 16 R01001

[54] https://www.aps.anl.gov/Beamlines/Directory/Details?beamline_id=27.

[55] *Advanced photon source safety assessment document*, Argonne National Laboratory, APS-3.1.2.1.0, Rev. 5 (APS_1188832).

[56] S.G. Arutunian, G. Decker, G.S. Harutyunyan and I.E. Vasiniuk, *Heat coupling in multi-wire vibrating wire monitor*, in *Proceedings of the 21st Russian Particle Accelerators Conference*, 28 September – 3 October 2008, Zvenigorod, Russia (2008), pp. 247–249.

[57] S.G. Arutunian, M.A. Davtyan and I.E. Vasiniuk, *Large aperture electron beam scan with Vibrating Wire Monitor in air*, in *Proceedings of the International Particle Accelerator Conference*, 23–28 May 2010, Kyoto, Japan (2010), pp. 876–878.

[58] M. Chung et al., *Double-wire vibrating wire monitor (dw-vwm) for beam halo monitoring in high-intensity accelerators*, in *Proceedings of 8th International Beam Instrumentation Conference*, 8–12 September 2019, Malmo, Sweden, pp. 373–376.

[59] J. Knaster, P. Garin, H. Matsumoto, Y. Okumura, M. Sugimoto, F. Arbeiter et al., *Overview of the IFMIF/EVEDA project*, *Nucl. Fusion* **57** (2017) 102016.

[60] S.G. Arutunian and A.V. Margaryan, *Oscillating wire as a "Resonant Target" for beam*, in *Proceedings of the International Particle Accelerator Conference*, 15–20 June 2014, Dresden, Germany (2014), pp. 3412–3414.

[61] S.G. Arutunian, M. Chung, G.S. Harutyunyan, A.V. Margaryan, E.G. Lazareva, L.M. Lazarev et al., *Fast resonant target vibrating wire scanner for photon beam*, *Rev. Sci. Instrum.* **87** (2016) 023108.

[62] M.A. Aginian, G.S. Harutyunyan, S.G. Arutunian, S.A. Badalyan, M. Chung, E.G. Lazareva et al., *Development of new algorithm in the method of a resonant vibrating target for large scanning speeds*, *J. Cont. Phys.* **54** (2019) 232.

[63] M. Aginian, J. Alonso, S. Arutunian, M. Chung, A. Margaryan, E. Lazareva et al., *New method in medical tomography based on vibrating wire: bench-test experiment on laser beam*, *J. Phys. Conf. Ser.* **826** (2017) 012016.

[64] E.G. Lazareva, *Vibrating wire for profile measurements of thin beams in particle accelerators: Preliminary tests using a laser beam*, *J. Cont. Phys.* **53** (2018) 136.

2021 JINST 16 R01001